The Effects of Neutron and Gamma Irradiation on Graphene

Christopher Nicholas Kryworuk

Thesis submitted to the faculty of the Virginia Polytechnic Institute and State University
in partial fulfillment of the requirements for the degree of
Master of Science
In
Mechanical Engineering

Mark A. Pierson, Chair
Scott T. Huxtable
Marwan Al-Haik

1-23-13
Blacksburg, VA

Keywords: Graphene, Neutron Irradiation, Raman Spectroscopy

The Effects of Neutron and Gamma Irradiation on Graphene

Christopher Nicholas Kryworuk

Abstract

Although young in its existence, graphene has already shown many potential uses in nuclear engineering. Graphene has unique electrical, mechanical and optical properties that give it unmatched potential for applications raging from sensors to composites. Before these applications can be fully developed, the response to neutron and gamma irradiation must be understood. In this study, graphene grown from chemical vapor deposition was irradiated by the High Flux Isotope Reactor at Oak Ridge National Laboratory and characterized using Raman spectroscopy. It was found that the amount of structural damage was minimal, but that the graphene was doped reversibly with H_20_2 and irreversibly. The irreversible doping is a type of soft etching process related to the exposure to O_2 as well as ionizations and heating caused by irradiation. The reversible doping is related to the products generated through the radiolysis of the water trapped between the sample and the substrate. By removing the water through evaporation the dopants related to the radiolysis products were found to be removed as well. These results are promising as they show that graphene is resilient and sensitive to the effects of irradiation simultaneously.

Table of Contents

Table of Figures

Table of Tables

1. Background and Introduction

1.1: Overview

This thesis will discuss the effects of neutron and gamma irradiation on graphene by using Raman spectroscopy. What graphene is, the process to make it and what Raman spectroscopy is and why it was chosen for characterization will be discussed in this chapter. In the next chapter the reasons why graphene was chosen and why it is important for irradiation research will be discussed. The following chapters will discuss the procedures as well as any related information for manufacturing, the High Flux Isotope Reactor (HFIR) and Raman spectroscopy. The final chapter will discuss the results and any conclusions from them as well as recommendations for future research.

1.2: Graphene

Ever since the discovery of carbon nanotubes by Iijima in 1991, research into carbon nanostructures has increased dramatically as they pose unique properties and offer a wide range of applications due to their small size [1]. Graphene, a monoatomic thick layer of sp^2 bonded carbon atoms has some of the most sensitive properties of all the carbon allotropes (carbon nanotube, fullerene, and diamond). Graphene consists of carbon-carbon bonds that have a spacing of 0.142 nm and form a two-dimensional

hexagonal honeycomb lattice with a thickness of a single atom [2]. If graphene sheets are stacked on top of each other they can form highly oriented pyrolytic graphite (HOPG). The graphene sheets in HOPG have a spacing of 0.335 nm and it is through the use of HOPG that many of the earliest experiments with graphene began [2].

It was the production of graphene through the use of scotch tape and HOPG known as mechanical exfoliation that helped Andre Geim and Konstantin Novoselov win the Nobel prize in physics in 2010 [3]. In this method, scotch tape was simply placed on HOPG, then pealed off and through the use of solvents monolayer graphene hundreds of microns long was able to be transferred onto substrates. However, this method was limited since graphene could only be produced on the micron scale and throughput was often low [3]. Larger and higher quality samples of graphene have instead been found to come from chemical vapor deposition (CVD) and the graphene used in this thesis is from the CVD process [2, 4].

1.3: Chemical Vapor Deposition

CVD is a technique known for thin solid film growth onto substrates through chemical reactions in the vapor species [4]. It consists of a gas delivery system, a

reactor and a gas removal system. The CVD system used for this experiment is shown in Figure 1.

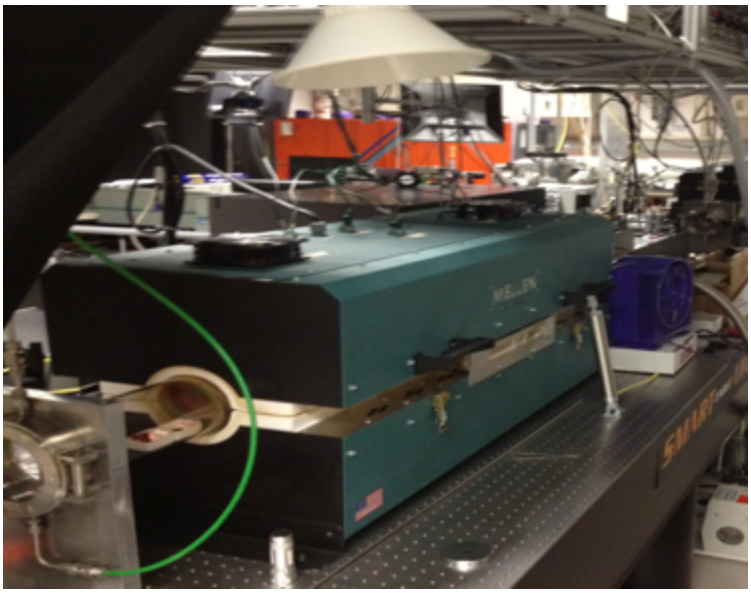

Figure 1 Shows the CVD system at ORNL used in this experiment. The reactor can be seen on the left hand side as the glass tube while the rest of the components including the heaters are within the enclosure. (Photo by author)

In the gas delivery system the necessary valves and mass flow controllers (MFCs) take the reactive gasses and uniformly mix them to the necessary flow rate before letting them into the reactor. In the reactor the necessary chemical reactions take place and the desired product is grown on the substrate. Heaters and fans often surround the reactor in order to achieve the right temperature needed for the reaction. This can be seen below in Figure 2. During and after the reaction the non-reacted gases and by-products are then removed by the gas removal

Figure 2 A CVD reactor shows graphene grown on a copper substrate. (Photo by author)

system, which consists of various pumps that keep the reactor at the right pressure along with gas removal. It should be noted that getting the precise flow of reactants and correct temperature and pressure for the correct reaction to occur is often difficult due to boundary layer growth and the complications from diffusion and convection [4]. Due to this it is particularly important to do several test runs and calibrations in order to produce the right products.

Along with having the right environment in the reactor, the requirement of having a catalyst, which lowers the energy barrier for the reaction, is extremely important. For the growth of graphene, the carbon solubility is an important metric of the catalyst. Copper

(Cu) has essentially zero carbon solubility and because of this is the most desirable catalyst in the growth of graphene [4]. If the catalyst were to not have zero solubility then carbon atoms would diffuse throughout the catalyst during temperature changes, which would affect the quality of the graphene. Another issue that catalysts introduce is the effect that grain boundaries can have on the growth of the graphene. The surface roughness of the catalysts, which is caused by grain boundaries, becomes an area in which carbon prefers to precipitate out on due to the higher surface energy these boundaries have. This causes thick graphene to form along these boundaries, which is usually not desired. To prevent this it is necessary to pre-anneal catalysts to reduce the size of the grain boundaries [4].

The two main issues of graphene deposited on a Cu catalyst are oxidation and strength of the etchant needed to remove the Cu from the graphene [4]. Compared to other catalysts such a nickel (Ni), Cu has a higher rate of oxidation that can cause a change to or damage the graphene that has formed on the Cu. To minimize oxidation, necessary precautions such as reducing the atmosphere exposure and the amount of time that the graphene spends on the Cu should be taken. During the transfer process from the

catalyst to the desired substrate strong etchants must be used to etch away the copper. Additional chemicals must then be used to remove the etchant. All of these chemicals may cause damage to the graphene and therefore great care must be taken during the transfer process. This transfer process will be covered in more detail under the procedure section of this thesis.

1.4: Raman Spectroscopy

One important tool for characterizing the damage and quality of carbon nanostructures is a process called Raman spectroscopy. Raman Spectroscopy works by sending monochromatic photons into an area of interest and relies on inelastic scattering to determine the condition of the lattice structure in the area. The photons interact with the phonons (molecular vibrations) and electrons which, depending on the bond type, will be re-emitted with either a lower or higher energy. By measuring this change in energy the type or lack of bonds in the area of interest can be determined [2, 5, 6].

What makes Raman spectroscopy such an important testing tool, is that it is non-destructive and one that can be run relatively quickly. Since the energy of a photon is proportional to its frequency, a Raman spectroscopy plot outputs the change in wavenumber of the

incident photon known as the "Raman Shift" in cm^{-1} on the X-axis vs. the intensity of the photon in arbitrary units on the Y-axis [6]. Approximately 1 in 10^7 of the incident photons are inelasticity scattered so the rest of the photons that are elastically or "Rayleigh" scattered must be filtered out as they do not provide any information about the vibrational modes of the system. The photons that are in-elastically scattered either lose energy (Stokes scattering) or gain energy due to the thermal phonons (anti-Stokes scattering) and are the ones that quantify the vibrational modes of the system which can be used to determine the condition it is in [7].

For all sp^2 bonded carbon allotropes such as graphene, there are three peaks in the Raman spectra that are indicative of the system's condition. These peaks occur under normal conditions at $1350cm^{-1}$, $1580cm^{-1}$ and $2700cm^{-1}$ and are known as the D, G and 2D-bands respectively [2]. The properties of these bands can change due to various factors as discussed below.

The most dominant of these bands is the G-band, which is related to the in-plane bonding of the carbon atoms and the doubly degenerated E_{2g} phonon mode at the Brillouin zone center. The Brillouin zone for graphene is an imaginary hexagonal cell that uses the carbon atom for its center and

is used as a unit cell for analysis. For graphene the G-band properties are affected by the dynamic effects of electron-phonon coupling. This means that changes in temperature and substrate can affect the wavenumber at which the G-band occurs. However, damage to the graphene or strain have a larger effect on the properties of the G-band much more than temperature or the substrate will. This is due to phonon propagation being more sensitive to the lattice structure itself, rather than the movement of the lattice structure [5-8].

The D-band, also known as the disorder band is attributed to the amount of disorder present in the system and is usually found in the range of 1250-1400cm^{-1}[6]. Pristine graphene samples should have no D-band present since graphene is periodic and has no disorder. However, with a fluence as low as 10^{11} Ar+ ions per cm^2, D-band formation has been observed in graphene samples and with an ion fluence of 10^{15} ions/cm^2 graphene has been shown to become highly disordered and nearly amorphous [9]. It is important to note that the energy of the incoming laser used can affect the wavenumber in which the D-band occurs. This relationship is $\frac{\partial w_d}{\partial E_{Laser}} \cong 50 cm^{-1}/eV$ for monolayer graphene with 1350cm^{-1} being the originating wavenumber for a 2.41 eV laser [6]. It is also important to note that this band will

keep on increasing with increasing disorder until the effects of damage start to coalesce and the sample becomes more closely related to amorphous carbon.[6]

Lastly, the 2D-band or sometimes called the G' band occurs roughly at twice the wavenumber of the D-band in the range of 2500-2800cm^{-1}. The iTO phonons, which propagate parallel with the lattice structure near the corners of the hexagonal lattice of the Brillouin (K-points), are responsible for this phenomenon. Much like the D-band, the 2D-band wavenumber is also related to the energy of the laser used by the equation $\frac{\partial w_{2d}}{\partial E_{Laser}} \cong 90 cm^{-1}/eV$ for monolayer graphene with 2700cm^{-1} being the originating wavenumber at 2.41eV. The 2D-band is sensitive to the sp^2 structure, which makes it an important tool for quantifying the number of layers in the graphene/graphite sample. This is due to the Lorentzian peak found in graphene, which causes the 2D peak to be ~3 times more intense than the G peak.

In addition to quantifying the number of layers, the 2D-band can also tell the stacking arrangement of the graphene sheets in graphite. If there are three layers or more of graphene, there can be up to 15 or more different scattering processes available for the 2D peak. This causes 15 or more peaks in the 2D wavenumber, which occur, so close to each other that they are usually

indistinguishable. This in turn causes the intensity of the peak to decrease as well, which is how the 2D peak can be used to discriminate the amount of layers found in a graphene/graphite sample [6, 8].

Since absolute intensities are generally not used unless the measurements can be taken on the exact same spot and closely in time to each other, ratios are often used instead [6-8, 10]. The reason why ratios must be used is that changes in absolute intensity can occur due to changes in atmospheric effects and are highly sensitive to any shifts in the mirror positions of the Raman machine while ratios are resilient to these effects [6, 7, 10]. In general the G/DD ratio is used to quantify the amount of layers of graphene in the sample. For single layer graphene the ratio should be ~0.3 with this value increasing as the number of layers increases [10].

In addition to the D-band alone, the development of disorder in monolayer graphene can be quantified by using the ratio of the intensity of the D-band to the intensity of the G-band. It has been found that this ratio increases with increasing L_D, which is the average distance between defects. This ratio has been empirically proven to approximate the average distance between defects L_a by the following equation:

$$L_a(nm) = 2.4 * 10^{-10} \lambda_{laser}^4 \left(\frac{I_D}{I_G}\right),^{-1} \quad (1)$$

where L_a is the characteristic size of crystalline sp^2 cluster structures, λ_{laser} is the wavelength of the laser used in nm, I_D is the intensity of the D-band in arbitrary units and I_G is the intensity of the G-band in arbitrary units [6]. It is important to note that this equation has empirically been confirmed to work well down to a L_a size of 2nm [11]. Scanning Tunneling Microscope (STM) imagining should also be used in conjunction with Raman spectroscopy to physically count the number of defects present in a sample. The amount of doping could also affect this ratio and cause the G/D ratio to decrease as well. In this research the two ratios that will be used for analysis is the G/D and G/DD intensity ratios.

2. Literature Review

2.1: Previous Related Research

Graphene is a two-dimensional substance, electrons behave as massless relativistic particles, which give rise to its unique electrical properties [12]. These properties include absence of localization and having the anomalous quantum hall effect occur at room temperature and the ability to act as a field effect transistor [13]. Graphene also has extremely high electron mobility at room

temperature (250,000cm^2/V-s), a Young's modulus of 1 TPa and thermal conductivity of 5000 $Wm^{-1}K^{-1}$ [2]. Normally graphene is a zero band-gap semiconductor, but by forming graphene into narrow 1-2 nm ribbons the band gap can be tuned such that graphene can be used as a transistor [14].

These exceptional properties give rise to many potential uses for graphene. As a result much research has been conducted into using graphene for: field effect devices, transparent electrodes, sensors, photodetectors, solar cells, energy storage devices, polymer composites and nanocomposites [2].

Although many of these uses are still far away, some of them are already becoming a reality.

One example of a practical use for graphene is its ability to detect a single molecule of gas [15]. By measuring the change of resistivity of graphene on a SiO_2 substrate, researchers were able to detect single molecules of gas coming in contact with graphene [15, 16]. Research has also shown that graphene resistance has a roughly linearly proportional relationship to disorder [11]. It was these two phenomena along with the unusual electrical properties that made graphene a strong candidate for use as a radiation detector.

2.2: Motivation for Research

As mentioned above, graphene has shown extreme sensitivity to any outside influences and has already shown single molecule detection abilities. Combined with a linear resistance response to disorder graphene could have a promising future in the nuclear engineering realm for detection. Before it can be used as a detector its resilience and response to irradiation must be known. This presents an issue as no research has been done on the response of graphene in a reactor type environment.

To date, most research performed on graphene has been done with low energy ions [9, 17-19]. The reason for this is that SEM, TEM and STEM microscopes use ions and electrons to map graphene and it was desired to find the threshold value of energy that could damage the samples in order to not exceed it during measurements. It was found that when using 500 keV C^+ ions that a total fluence of $5*10^{13}$ ions/cm^2 was needed before the total loss of graphene's unique electrical properties occurred [18]. However, the properties of graphene were found to change on the Raman spectra with a fluence as low as 10^{13} [18]. Research has also been performed with 2.0 MeV proton irradiation and showed monolayer graphene to have a threshold fluence of $1*10^{16}$ ions/cm^2 before any change in the Raman plot was noticed with disorder occurring at 10^{19} [20].

Although these studies provide a decent introduction as to how graphene would respond under irradiation they lack a wide range of energies and also any information on the effects of gamma and neutron irradiation. To date no empirical measurements have been conducted with either gamma or neutron irradiation, only simulations have been done. One simulation found that the maximum energy of an ion or neutron needed to potentially displace a carbon atom from graphene was only 0.18eV [21]. The study also found that in simulations, the graphene sheet went from metallic to semi conduction providing yet another potential phenomena for graphene to be used as a radiation detector [21].

Lastly, a group in Purdue University is also trying to use graphene for the detection of radiation, specifically gamma rays and neutrons. By applying a voltage gate to graphene separated by an insulator and an undoped semiconductor on the bottom such as Si, SiC and GaAs a change in resistance was found after an X-ray flux. Over a 50% change in resistance was found from the X-ray flux of 15kV and 15μa to one of 40kV and 80μa. This change in resistance is due to the field effect transistor properties of graphene and was caused by ionizations in the undoped substrate[22, 23]. A similar device using boron for neutron

absorption below the Si semiconductor has also been tested and shown to have some success in measuring a change in resistance after irradiation from an Am^{241} source [22, 23]. In both cases measurement of the effects on graphene itself have not been measured directly.

Along with being used as a potential sensor in a radiation environment, graphene has also been researched for the purpose of nanocomposites and space shielding [24, 25]. For these reasons it is imperative that the effects of a wide range of radiation and in particular the effects of neutrons and gamma rays must be measured. By knowing the effects of these particles new ways to exploit graphene as a potential radiation sensor along with additional uses for graphene may be found. Due to the strong material properties yet sensitive nature of graphene, it is believed that it will excel as a radiation detector and could one day become a standard for radiation detection.

3. Synthesis Procedure

3.1: Introduction

As discussed in the background graphene is carefully grown on a copper foil substrate using a CVD process. Since this process is proprietary to Oak Ridge National Laboratory (ORNL) specifics such as flow rate, pressure, temperature and time in the CVD reactor cannot be discussed. What will be discussed are the steps taken to transfer the graphene from the copper foil to the silicon-silicon dioxide substrate, the irradiation procedure and the specifics of the Raman measurement procedure.

3.2: Substrate Choice and Preparation

Before conducting the experiment much thought was put into making sure a viable substrate was chosen. Due to the high neutron flux in the high flux isotope reactor (HFIR), many substrates become too radioactive after being exposed leading to a long decay period that in some cases could take many years before the sample could be released as nonradioactive. Along with having to be resilient to the radiation levels the substrate must also be suitable for graphene transfer and if possible provide adequate contrast so that the graphene can be seen with a normal microscope under normal white light conditions. Lastly, the substrate must enhance the Raman signal of monolayer graphene as the wrong type of substrate can cause graphene to become

undetectable [26]. After much thought it was found that a silicon-silicon dioxide substrate would be the best compromise for these criteria.

Naturally occurring Silicon is composed of three isotopes: Si-28 (92.23%), Si-29 (4.67%) and Si-30 (3.10%). Of these three isotopes Si-30 provides the biggest issue as it becomes radioactive after absorbing a neutron and becoming Si-31 [27]. Fortunately Si-31 has a short half-life of ~157 minutes and undergoes beta minus decay with a ~1.5 Mev electron on average [27]. Although this beta particle is not ideal for this experiment, it is believed that the relatively high energy of the beta particle will cause it to pass through the graphene sample with only minor ionizations [19]. This is due to the increasingly low interaction cross-section that the carbon atoms have as the beta particles increase in energy in addition to the increasingly shorter interaction time [19]. The low concentration of Si-30 in naturally occurring silicon also helps minimize the amount of damage caused by the beta particles.

In order to help visualize and locate the graphene on the silicon, a silicon dioxide thickness of 300nm was chosen. At this thickness an optical resonance is created that enables single layer graphene to be seen with a normal

microscope [28]. The thickness of the oxide layer on the silicon must be exactly at this value because deviations as small as 5% have been shown to make this phenomena disappear [28]. Changing the light used for illumination on the sample can alleviate this, but for normal white light

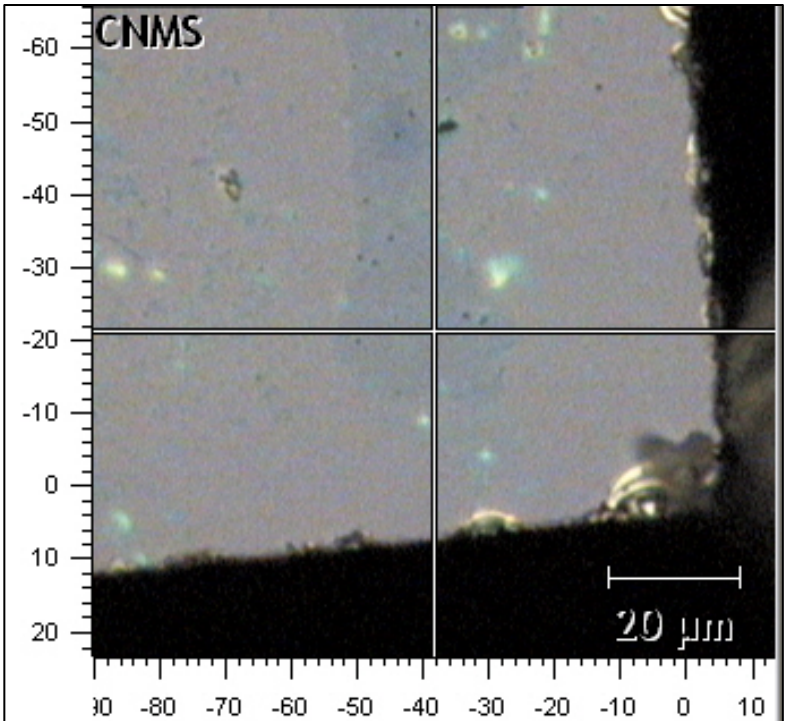

Figure 3 Shows the graphene against the $SI0_2$ substrate. The graphene appears darker than the rest of the substrate and is pointed out by the crosshairs. (Photo by author)

an oxide thickness of 300nm must be used. An example of this phenomenon can be seen in Figure 3.

It should be noted that due to the precise thickness of the oxide required, P-doped silicon had to be purchased. The particular P-doped silicon that was available was doped with boron, which does present some issues while being under neutron irradiation. Although no energetic beta or

gamma particles are produced from the boron, neutron induced heating can occur. Since boron has an extremely large scattering cross section for neutrons, neutrons bounce off the boron atoms and deposit some of their momentum as they hit. This deposited momentum produces heat, which can be an issue at higher fluences. Due to this neutron induced heating all irradiation times must be kept under five minutes. If this threshold value is breached then the boron induced heating can cause the sample to completely disintegrate and become a powder. Along with enhancing the visible optical signal, the silicon-silicon dioxide substrate also enhances the Raman signal of the graphene, this is known as interference-enhanced Raman scattering (IERS) [26].

Lastly the substrate had to be sized correctly so that

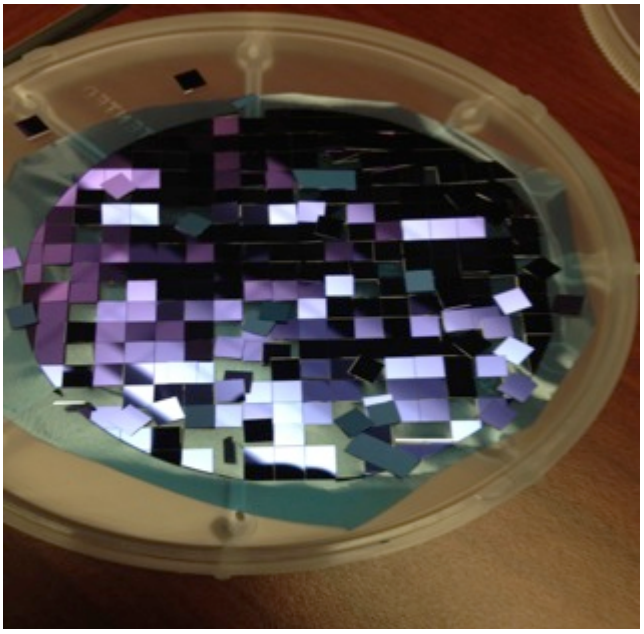

Figure 4 The original silicon wafer has been cut into hundreds of smaller pieces. This was by the disco dicer. The original shape of the wafer can still be seen. (Photo by author)

it could fit in the "Rabbits" used in HFIR. To achieve this, a disco dicer was used to cut the normal silicon wafer into 0.5 cm by 0.5 cm pieces. The end result of this procedure can be in Figure 4. This was done in a clean room to prevent potential contaminants from forming onto the substrate. It should be noted that a scribe method was initially used to try and reduce the wafers to the correct size. This proved to be inadequate as the pieces disintegrated and were harder to manage as they became smaller.

3.3: Graphene Transfer

After the graphene samples on copper were received from the CVD reactor and the substrates were prepared the transfer process was initiated. First the copper was cut up

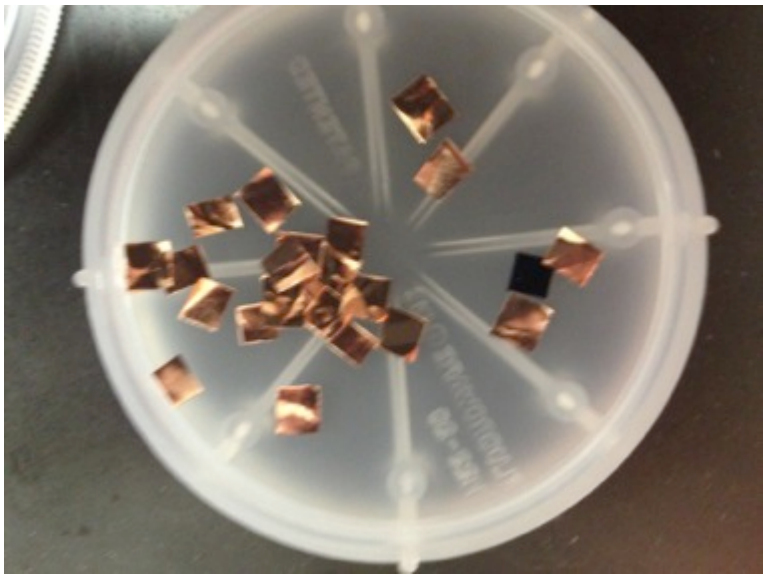

Figure 5 Graphene on cut copper pieces. (Photo by author)

into smaller pieces as shown in Figure 5. Originally these pieces were much larger. Raman spectroscopy was used to verify which side of the copper the graphene was on. After verifying the existence of the graphene on the cooper pieces, they were cut as shown above to match the size of the silicon-silicon dioxide substrate. The pieces of copper were then attached with double-sided tape to a rotation device. After they were attached two drops of Poly-methyl-methacrylate (PMMA) were dropped in the middle of the

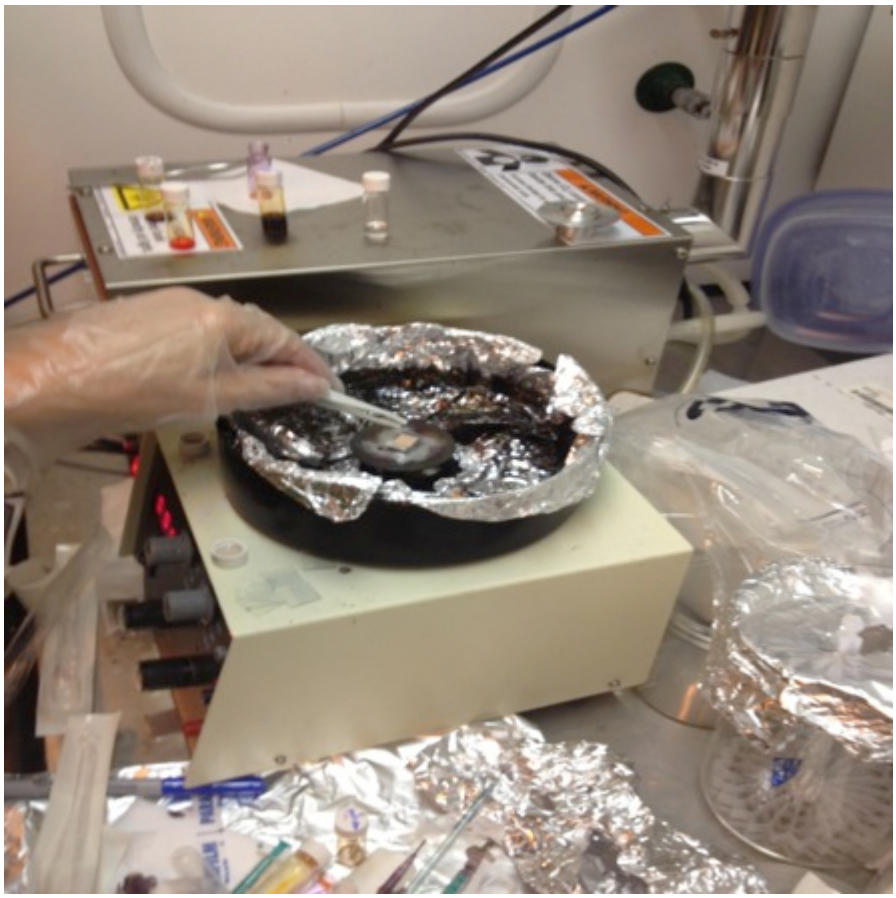

Figure 6 The device used to rotate the PMMA on the cooper. (Photo by author)

copper on the side with the graphene and it was then

rotated at 4,000 RPM for a couple of minutes to make sure that a thin even coating was applied across the sample. This device is shown above in Figure 6.

After the PMMA was applied to each sample, each sample was then placed on a hot plate for 2 minutes at 170°C to remove all the excess PMMA left on the sample along with the residue left from the double sided tape. This process can be seen below in Figure 7

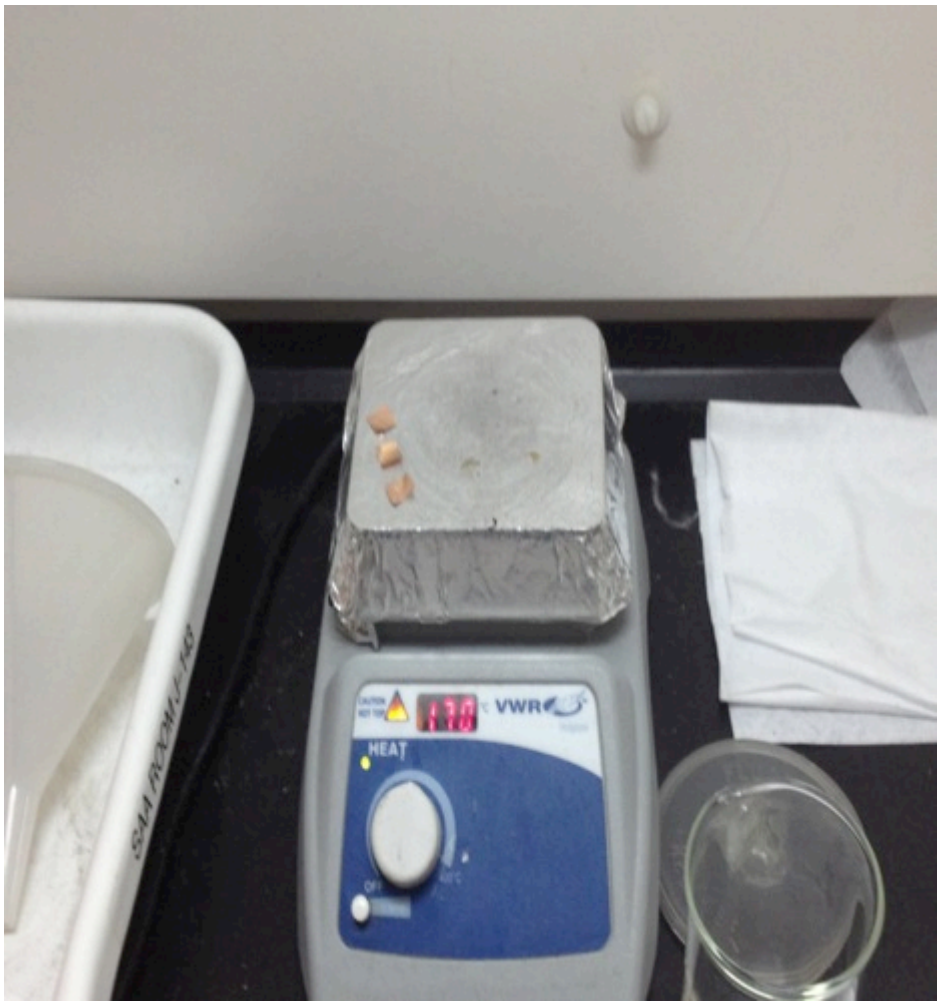

Figure 7 Shows the hotplate used to remove the excess materials. (Photo by author)

After the excess materials were removed, the samples were then placed in a solution that contained 5 grams of ferric nitrate per 100ml of water. It is important that the PMMA side of the samples was placed upward and that the samples floated in this solution. What this solution will do is etch away the copper such that only the PMMA and graphene will remain afterwards. In order to prevent samples from coming in contact with each other, each sample had to be placed in a disc with a four-way divider to prevent each sample from coming in contact with each other. The setup used can be seen below in Figure 8.

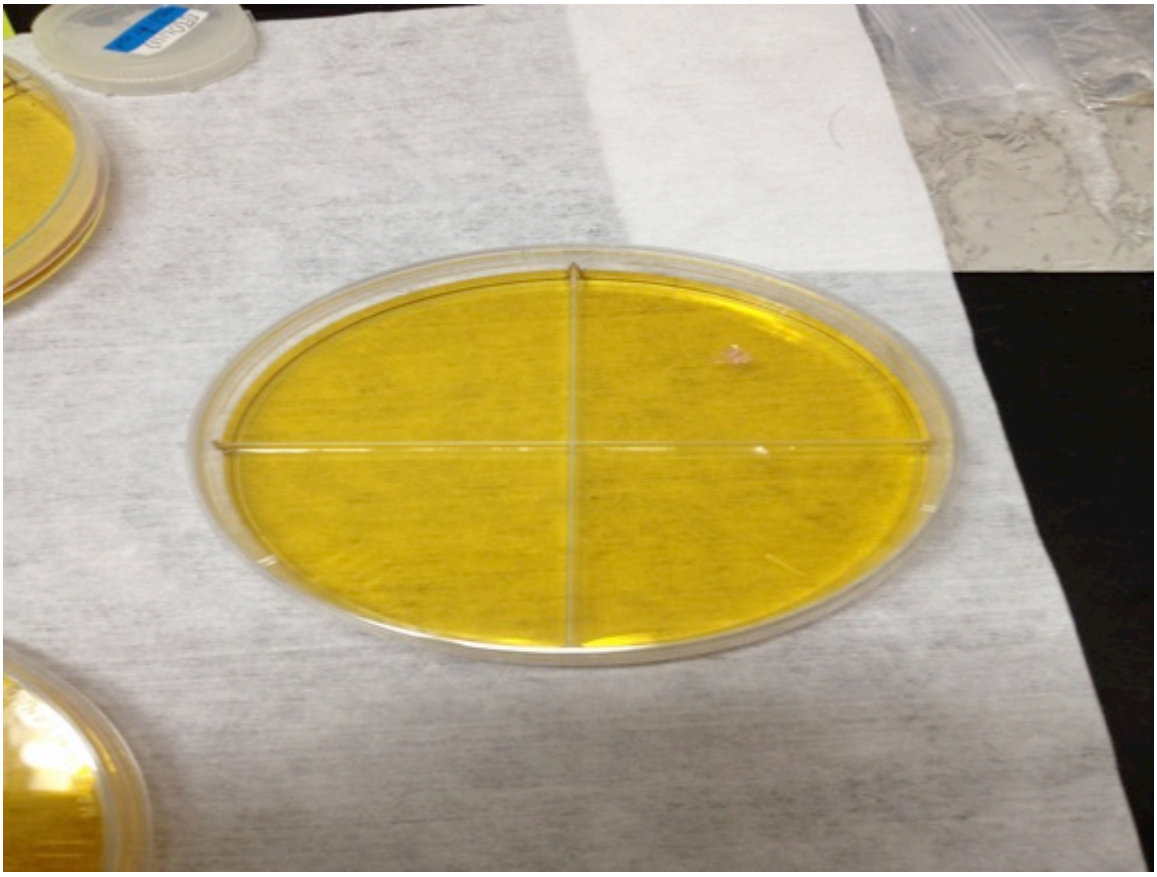

Figure 8 A piece of copper etching away in the solution can be seen in the top right (Photo by author)

The samples were left in this solution for at least four hours so that all the copper could be completely etched away. After the copper had completely etched away, the floating PMMA/graphene was then carefully picked up with a glass slide and placed in de-ionized water. Similar to the previous chemical mixture, the PMMA/graphene will float on the de-ionized water due to the surface tension. Unfortunately, due to the lack of copper now present in the mixture it was impossible to capture a picture that showed the graphene/PMMA clearly floating on the de-ionized water. Great care was taken to make sure that the PMMA side was still pointing upward and that the sample was not folded as it was transferred onto the de-ionized water. Although it was difficult to capture with a camera, the floating PMMA/graphene was still visible with human eyes under normal lighting conditions.

After the PMMA/graphene was located, it was then picked up with the silicon-silicon dioxide substrate, using tweezers and much care. A “swimming” motion was used to get the substrate under the sample and then it was carefully picked up. This can be seen in Figure 9 below.

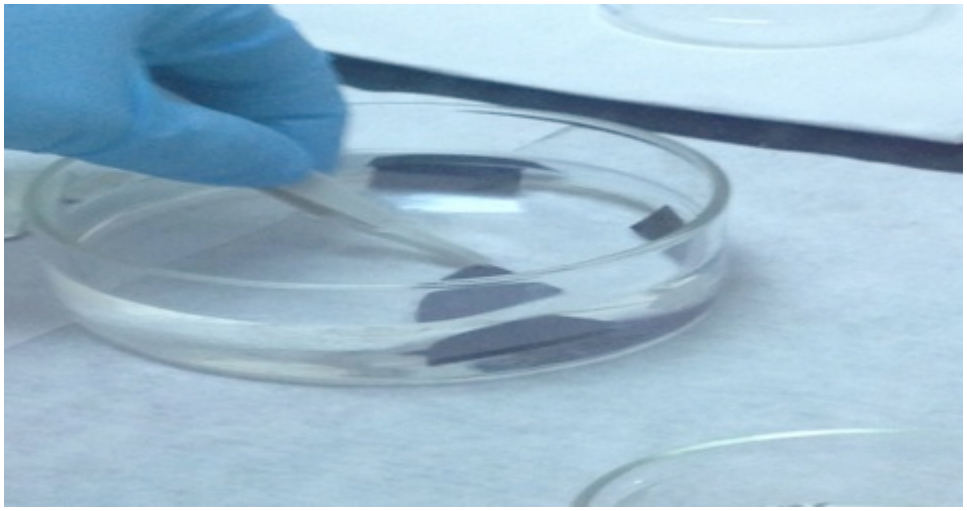

Figure 10 Shows the process of scooping up the PMMA/Graphene from the water. Note that the substrate shown in this figure was much larger than the substrates used for irradiation and was simply for practice. (Photo by author)

After the PMMA/graphene was picked up and placed on the silicon-silicon dioxide substrate, it was then placed on its side to increase the rate of evaporation of the remaining de-ionized water on the sample. The sample was left like this overnight to ensure all the water had evaporated, This is critical before further purification as

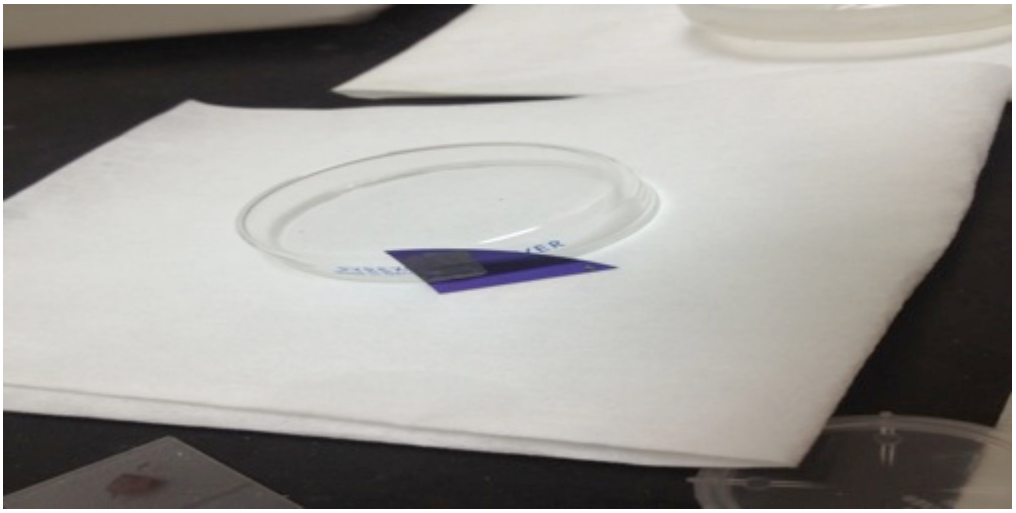

Figure 9 Shows the PMMA/graphene that is attached to the silicon-silicon dioxide substrate placed on its side to allow all the remaining water to evaporate. As in the previous figure this substrate is much larger than the one used in the final irradiation. (Photo by author)

any remaining humidity can greatly affect the removal of PMMA. This process can be seen in Figure 10

After all the water had evaporated from the sample overnight, the sample was then placed in acetone for 10 minutes and then methanol for approximately 30 seconds. This removes all the remaining PMMA from the sample and leaves just the graphene and silicon-silicon dioxide. The

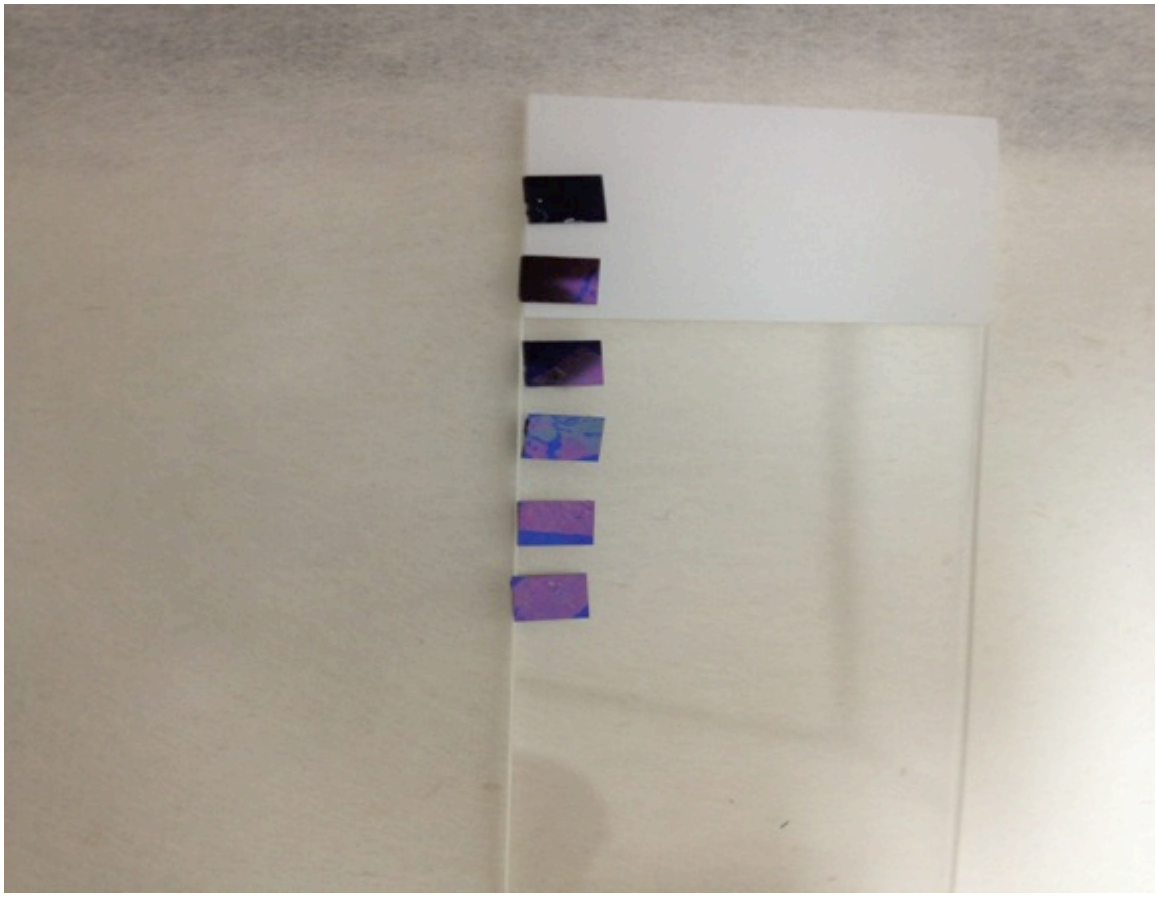

Figure 11 Shows the final result of the transfer. Note that the 1cm by 1cm squares shown above are the correctly sized substrates for irradiation. (Photo by author)

final product can be seen in Figure 11. It should be noted that the dark purple areas of the sample are where the graphene is not attached to the substrate while the lighter

purple/greenish areas of the sample are where graphene is present.

After using Raman spectroscopy to verify the presence of graphene on the sample, the 1cm by 1cm graphene/silicon-silicon dioxide squares were placed inside HFIR for irradiation. It should be noted that graphene is highly sensitive to ozone and can be damaged by simply being exposed to it [29]. To minimize the effects of ozone on the graphene samples, the samples were kept under vacuum when not in use as Figure 12 shows. Although the vacuum chamber at HFIR is different from the one shown above the same general principles still apply and all samples were kept in a vacuum at all times while not being irradiated.

Figure 12 Shows an example of one of the vacuum boxes used to minimize the effects of ozone on the samples. (Photo by author)

4. The HFIR Procedure

4.1: The HFIR Introduction

After the samples were processed as described above and looked like Figure 11, Raman spectroscopy was performed to double check the graphene coverage before irradiation. This process will be discussed further in the following section, but this section's focus is to discuss how the irradiation procedure was performed and how much radiation the samples were exposed to along with a brief description of the HFIR facilities.

4.2: The HFIR Background

The HFIR is a research reactor located in ORNL that operates at 85 MW and was chosen due to having the highest average thermal neutron flux in the US, of 2.3×10^{15} neutrons/cm^2-second in addition to being located near the Center for Nanophase Materials Research (CNMS) [30-32]. Since the objective of this research was to study the effects of neutron damage on graphene, this high neutron flux was desirable to help make more probable the damage caused by the neutrons rather than the other forms of beta and gamma radiation that are found in all nuclear reactors. The close proximity of CNMS was also beneficial as it cut down on travel time and allowed measurements to be performed right after the samples were released. The HFIR operates on highly enriched uranium-235 fuel and is

designed as an annular fuel assembly that has several different concentric cylinders that each serve a unique purpose. This design can be seen in Figure 13.

Due to location of the beryllium reflectors, the highest

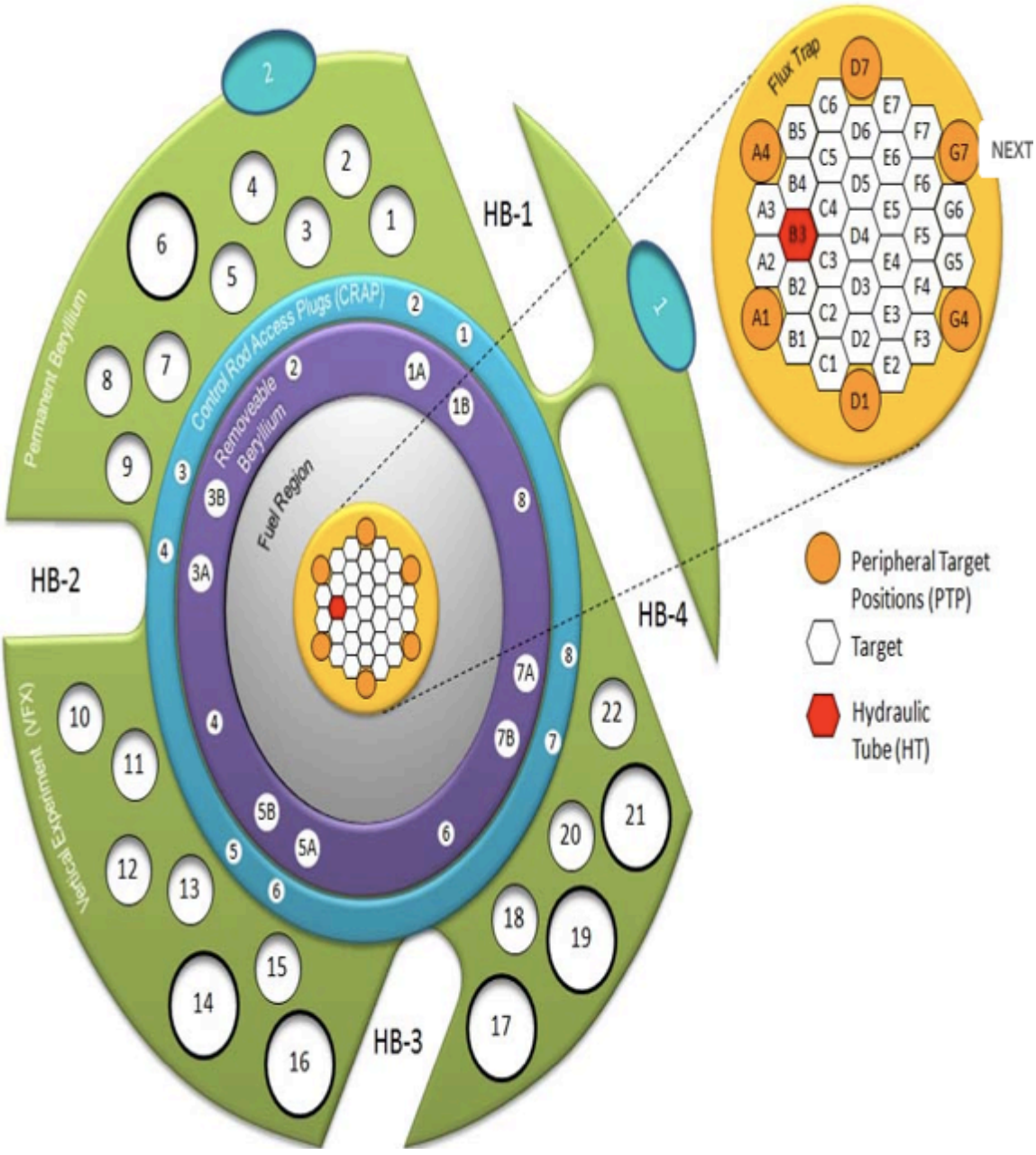

Figure 13 The layout of HFIR with possible measurement locations can be seen. [32]

fast and thermal neutron flux are located toward the center of the reactor while the outer layers of the reactor have a lower fast and thermal neutron flux. Since one objective of the research was to try and find a threshold fluence that generated detectable damage, the lowest possible neutron flux was desired. Due to this, the pneumatic tube facilities shown as spot 1 and 2 in Figure 13 above were chosen as irradiation spots. The pneumatic tube facilities allow irradiation times as low as ~5 seconds and could theoretically be used the for up to reactor fuel life of ~26 days [30-32]. The amount of thermal and fast neutrons that the samples are exposed to across HFIR can be seen in Figure 14 below.

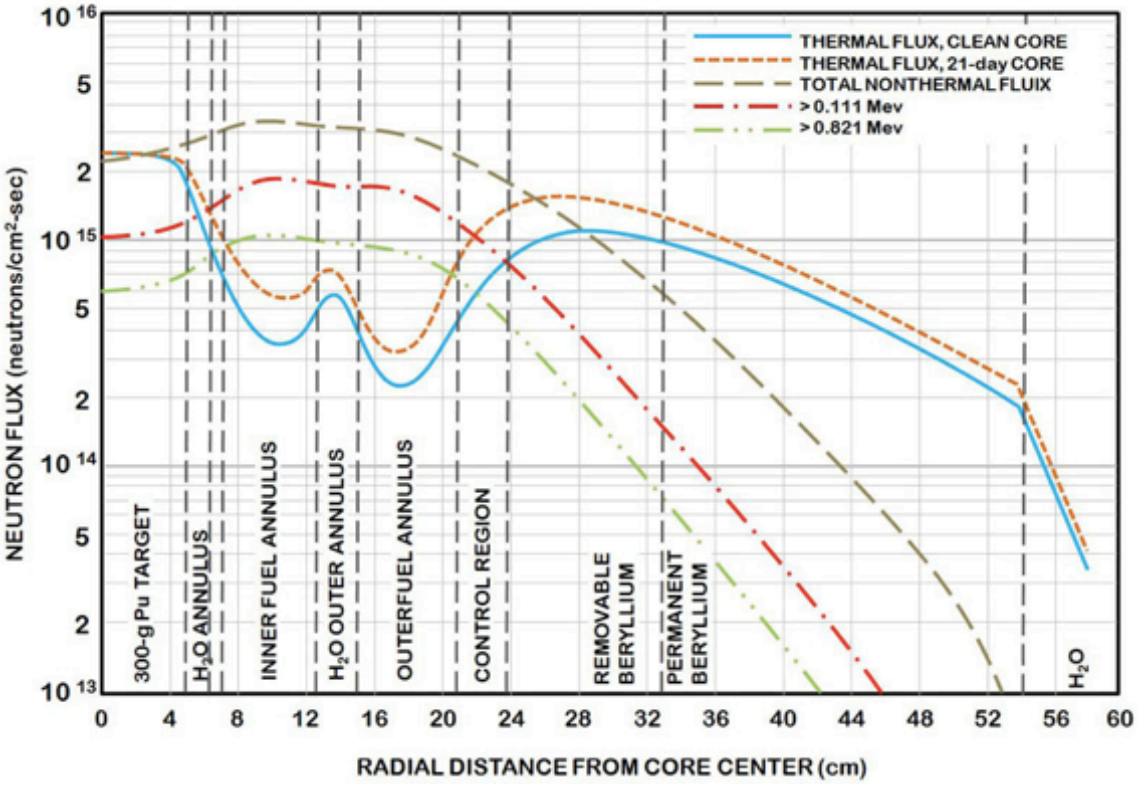

Figure 14 Shows the thermal and fast neutron flux changes across HFIR. Note the samples were located roughly 48 cm from the center. [32]

Of the two pneumatic tube facilities PT-1 and PT-2, PT-2 has the lower average thermal neutron flux of 4.00 x 10^{13} compared to 4.32 x 10^{14} neutrons/cm^2-second for PT-1 [32]. However, PT-1 was chosen as it has a lower irradiation time potential and access to the neutron activation analysis (NAA) labs. Access to these labs is necessary because in order to conduct measurements at CNMS, samples must be free of any detectable irradiation. This clearance can only be done in the NAA labs.

4.3: HFIR “Rabbits” and “Carrots”

The PT-1 pneumatic tube facility works much like a pneumatic tube at a bank drive-up teller and uses air to move around a cylindrical “rabbit” from HFIR to the NAA lab. The rabbit is made from high density polyethylene (HDPE) and has an outer diameter of 14.48 mm and an inner diameter of 9 mm with a height of 18 mm. The rabbits are manufactured by the NAA laboratory group and through experimentation were found to be able to withstand the heating that occurs in HFIR for the fluence times of this experiment. To minimize the amount of damage due to the roller coaster like path that the rabbits take through the HFIR, small cylinders called “carrots” were placed inside each rabbit. Each carrot is 8.75 mm in diameter and 2.5 mm tall and fit snuggly in the rabbits. The rabbits and carrots can be seen below in Figure 15. The carrots are made of the same HDPE as the rabbits and therefore much like the rabbits are able to withstand the temperatures reached in HFIR for this experiment. Due to this durability, out gassing which could affect the Raman measurements is not existent at the fluences of this experiment.

Figure 15 Shows the rabbit and carrot next to a quarter for scale. (Photo by author)

4.4: The Gamma Facility

Along with being able to provide neutrons for experiments, the HFIR facilities also are able to provide gamma rays for experiments that wish to study the effects of gamma rays exclusively. The gamma rays were produced from the spent fuel from the HFIR. Due to the wide range in age found in the spent fuel assemblies a relatively wide range of dose rates are available, the largest of which being ~$1.8*10^{8}$ rad/hr. The gamma facility has a cylindrical sample holder that has a 3.75″ diameter and is 25″ long which allows for much larger samples than the PT-1 facilities [32]. These facilities were used to try and de-couple the effects of the gamma irradiation from neutron irradiation. In order to make sure that circumstances were

similar to the HFIR a special “umbilical” cord was used to pump air in the container, as the container is kept underwater in a spent fuel pool. Usually inert gasses such as argon and nitrogen are used in order to prevent any combustion, but since the rabbits did not have these inert gases available, air was used instead to mimic the environment found in the HFIR.

4.5: Neutron and Gamma Irradiation Times

By using a process of trial and error it was determined that for boron doped Si-$Si0_2$ the longest irradiation time possible was ~300 seconds, as any sample that was over this time became too radioactive to be releasable in a reasonable time. The isotopes responsible for this radioactivity were Cr-51 and Ir-192 and it is assumed that these impurities came from the Si-$Si0_2$ substrate, as none of these isotopes are thought to be present in graphene or the materials used to make graphene. The neutron irradiations were conducted on July 3rd 2012 and afterwards were kept under nitrogen until August 28th 2012 when the Raman measurements were conducted. After doing spot measurements with Raman spectroscopy it was determined that ~30 seconds was the threshold value in which the effects of radiation could be measured. Due to the low quantity of high quality graphene samples available, only

four irradiation times could be used. These irradiation times were: 30, 60, 100 and 300 seconds. By using the average neutron flux of $5.44*10^{14}$ n/cm^2-sec which was found using a 238 group Monte Carlo simulation across the energies of $1*10^{-11}$ MeV to 8.19 MeV and provided by the HFIR staff the corresponding fluences shown in Table 1 below were calculated [33].

Table 1 The total fluence for each sample

Sample	Irradiation Time (sec)	Fluence (n/cm^2)
1	30	$1.63*10^{16}$
2	60	$3.27*10^{16}$
3	100	$5.44*10^{16}$
4	300	$1.63*10^{17}$

It should be noted that originally a sample had intended to be irradiated for 200 seconds, but due to some high levels of contaminates found in the sample, the sample was unable to be released. It should also be noted that while being irradiated it was estimated by the HFIR staff that the maximum temperature the samples reached due to gamma induced heating was ~250°F. The effects of this temperature will be discussed further in the following section. In order to simulate the gamma dose that samples experienced in the HFIR a conversion rate was provided by the HFIR

staff. This conversion rate was $9.766*10^8$ rad/hr and was found in MCNP using an air dose approximation [33]. It should be noted that since the gamma flux in the spent fuel has less energy on average, more time must be spent in the gamma facility compared to the HFIR facility. The gamma irradiations were conducted from November 29-30th 2012 with the spent fuel element from cycle 444 in LS-1 and then placed in a vacuum until December 4th when the Raman measurements were taken. The total does and amount of time each sample was exposed to are shown in Table 2 below.

Table 2 Total dose for each sample

Sample	Irradiation Time HFIR (sec)	Irradiation Time Gamma (sec)	Requested Dose (rad)	Actual Dose (rad)
1	30	1380	$8.138*10^6$	$8.14*10^6$
2	60	3000	$1.627*10^7$	$1.73*10^7$
3	100	4440	$2.712*10^7$	$2.71*10^7$
4	300	13320	$8.138*10^7$	$8.14*10^7$

It was requested of the HFIR staff running the gamma facility that the maximum temperature not exceed 250°F as it was undesirable to have a temperature that exceeded the one assumed in the HFIR irradiation.

4.6: Sample Heating and Control

In order to simulate the heating effects that the samples underwent while being irradiated in the gamma

facilities and the HFIR, an oven was used. Due to the low amount of high quality samples only one sample could be kept for heating. To be conservative, this sample was heated to 300°F for 300 seconds, which is 50°F higher than the maximum temperature that occurred during either irradiation and is the maximum time spent in the HFIR. Unfortunately this experiment was conducted before finding out that there would be an extreme difference in irradiation time for the gamma and the HFIR samples and due to a lack of samples available the experiment could not be repeated. However, it should be noted that although heating time is important, current research shows that the maximum temperature is much more important, as there is a threshold temperature which is well over 600°F in which any type of annealing or damage can occur and below this temperature structural changes to graphene should not occur [34, 35]. The sample was also placed in a “carrot” to fully simulate the environment in the HFIR. Figure 16 below shows the oven used for the simulation of the heating. After the heating of the sample was finished, the sample was immediately placed in a vacuum box to prevent any issues with atmospheric exposure.

Figure 16 The oven and the container used can be seen. Although the container used in this experiment is larger than the "carrot", it is made of the same HDPE. (Photo by author)

As discussed in the graphene transfer section, all samples were kept in either a vacuum or in inert gasses when not in use. This was done to prevent the effects that the atmosphere could have on the samples. This is vital due to the relatively short time that the ozone in the atmosphere needs in order to damage the samples. The control sample was also kept in a vacuum box for the duration of the experiment and had a measurement done initially and then at the end of the HFIR irradiations. This period was such that the time between the measurements was the same as the time between the measurements for the HFIR samples.

5. Raman Spectroscopy Procedure

5.1: Raman Spectroscopy Introduction

As mentioned previously, Raman spectroscopy is widely considered one of the best non-destructive methods for quantifying change in nano-carbon structures [2, 5-8]. The Raman spectroscopy machine used for this experiment was a Renishaw Micro-Raman machine, which can be seen below in Figure 17. The Raman system has a coordinate system, attached video camera and has a wide range of settings for conducting measurements. The settings used in this experiment along with the procedure taken to make each measurement will be discussed further in the following

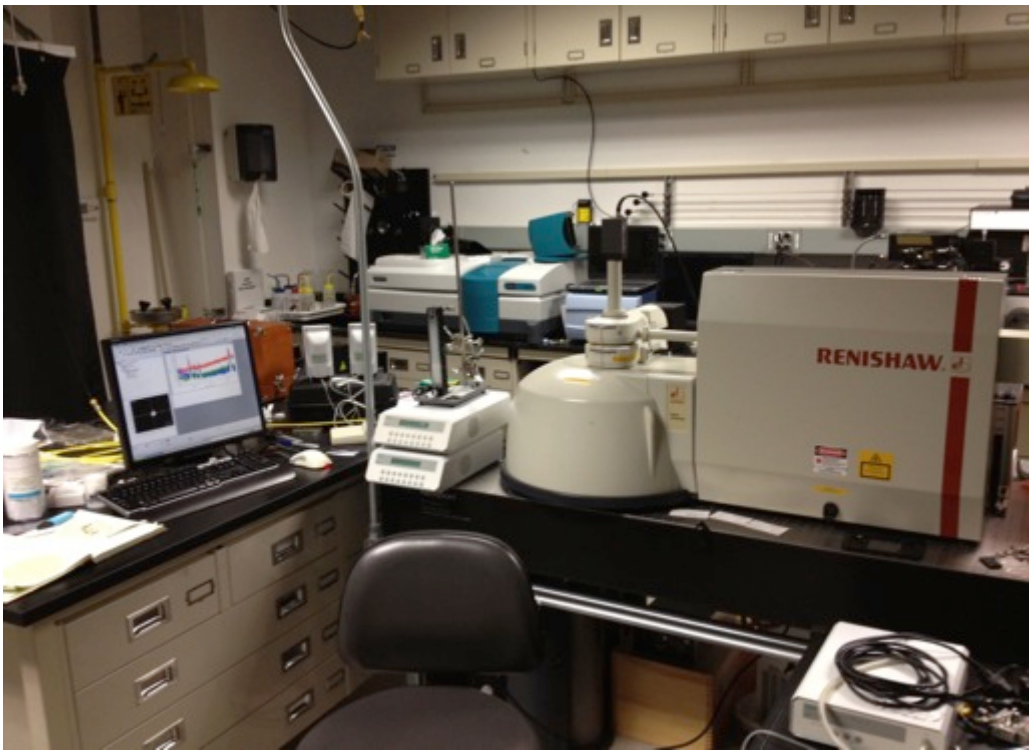

Figure 17 The components of the Raman spectroscopy system can be seen. The Renishaw box on the right reflects a laser onto the sample in the conical sample holder. (Photo by author)

sections.

5.2: Establishing a Coordinate System and Origin

Due to the high variability found in the samples, it was critical that the same area was being investigated before and after irradiation. In order to do this a coordinate system had to be established along with a method to replicate the same origin. The first step of this process was using a straight edge and drawing a line on the glass slide so that the samples could be placed at roughly the same angle each time. An example of this can be seen below in Figure 18.

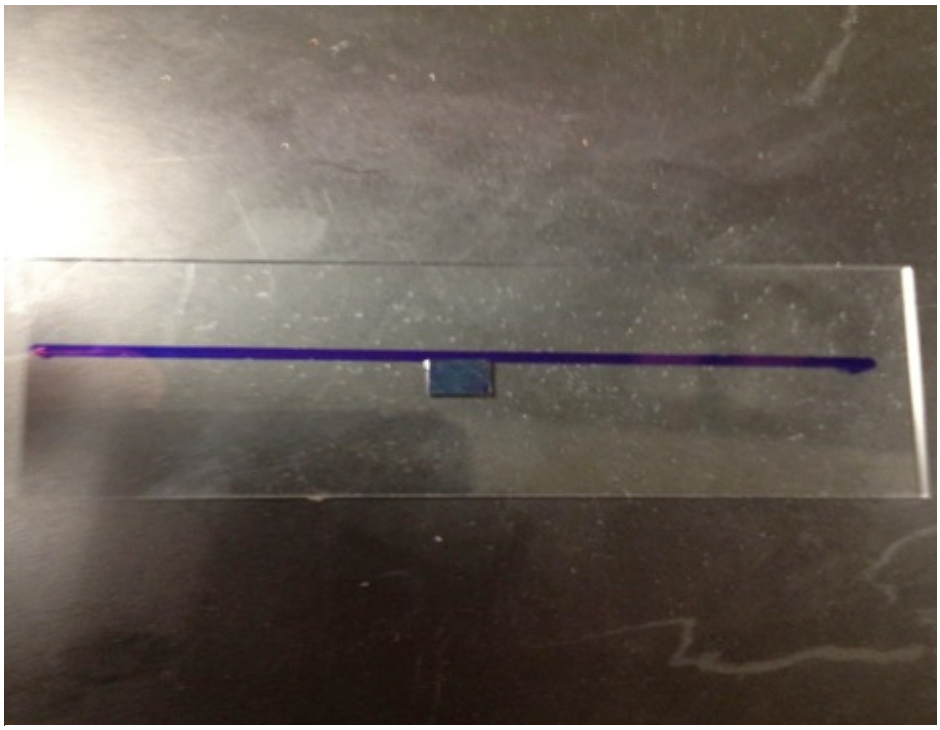

Figure 18 A marked glass slide with a sample placed and ready for measurement is shown. (Photo by author)

Although this process did not translate to precision on the micrometer scale, which was necessary for these

measurements, it did greatly reduce the amount of time needed to get within the necessary limits. Along with marking the glass slide used in the measurements, a small dot was made on the bottom right corner of the backside of each sample. This mark was made with a normal Sharpie mark, which does not come off during irradiation nor produce any radioactive isotopes after irradiation. This marker was critical, as it made sure each sample was oriented in the same manner before and after irradiation. After all Sharpie marks were made the sample was ready to be placed under the Raman machine's microscope.

However, if it was the first sample of the day to be measured a calibration was necessary. This calibration was performed using a designated piece of silicon and the quick calibration feature in the Renishaw software. The main metric of the calibration was to make sure that after running the calibration the resonant peak found in silicon occurred within 1 cm^{-1} from the normal peak position, which is 520.5 cm^{-1}. If the resulting plot did not look like Figure 19 below then more calibration would be necessary. This further calibration could be simple measures such as dusting using canned air all the way up to more complicated tasks such as realigning the mirrors found in the Renishaw box. Most of the time a quick calibration was all that was

necessary. After the calibration was performed the sample was then finally ready to have a coordinate system put in place.

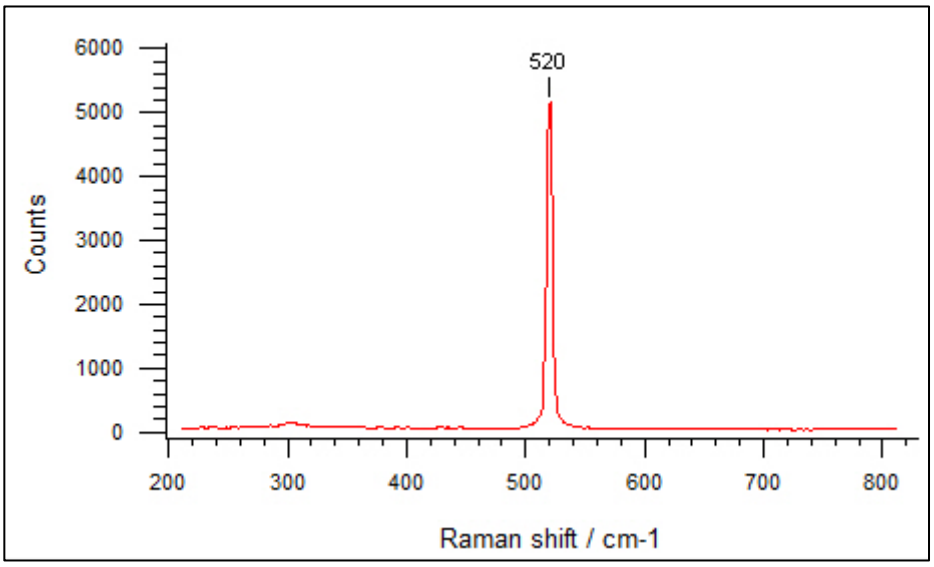

Figure 19 A calibrated Raman plot of silicon with the proper resonant peak is shown. As mentioned in the background counts are in arbitrary units. (Plot author)

The first step that was taken after the sample was placed in the microscope was to find the bottom right corner of the sample. After this was done the origin was set and a picture of this new origin was taken for future reference. This picture was critical, because as Figure 20 shows even with knowing to set the origin to the bottom right hand corner the exact point of this "corner" becomes difficult to define under extreme magnification and having the origin off by a couple of micrometers between measurements could drastically effect the location of the map performed. So to prevent this, extreme care was taken

to adequately document the origin and area around the origin.

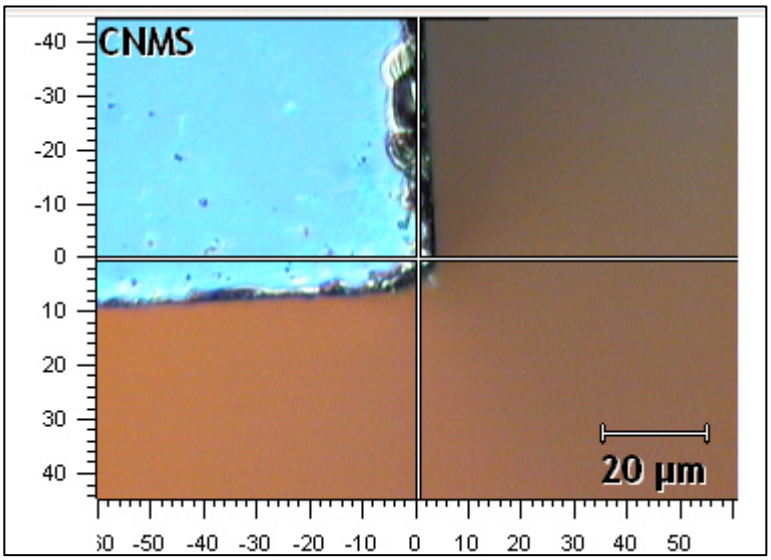

Figure 20 The origin under a 50x objective is being set for a sample. Notice the lack of a definite "corner". (Photo by author)

It should be noted that just before the origin was set, the sample was rotated such that the crosshairs ran parallel to the two edges of the sample as much as possible. This was done by moving the glass slide and not the sample itself so that the sample would still be aligned with the Sharpie mark on the glass slide. By combining these two techniques the repeatability of the coordinate system was maximized.

5.3: Mapping Locations and Documentation

After the origin had been set and the coordinate system established, a suitable area for mapping had to be found. When choosing an area to map three key factors were used to narrow down potential locations. These factors

were: quality and quantity of graphene, proximity to origin and proximity to a distinguishing feature. However, before a map location was determined a montage was generated for further documentation and location purposes. An example of an average montage generated can be seen in Figure 21.

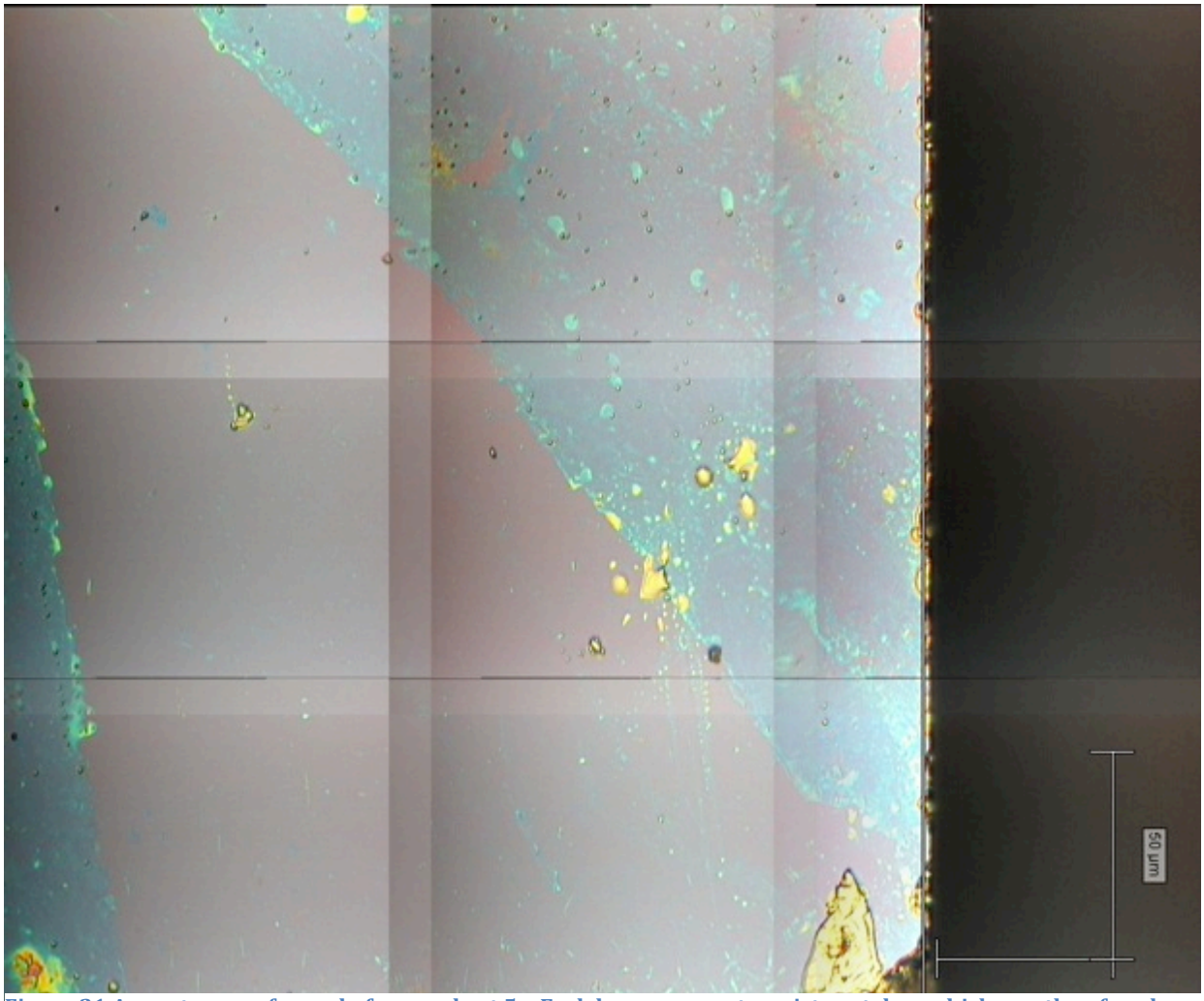

Figure 21 A montage performed of a sample at 5x. Each box represents a picture taken which was then fused together in the imaging software to form the montage. (Photo by author)

The montage was generated for multiple reasons. It provides a clear overview of the sample near the origin and since the graphene can be seen with a bluish tint, the montage allows for a potential mapping area to be quickly

identified. The montage also helps document the sample and provides a map that allows for easy location of a specific area based off of a certain feature such as a gash or graphene gradient. This is particularly useful for post irradiation measurements when the coordinate system alone is not enough to locate the same mapping region used before.

As mentioned above the area used for mapping was kept close to the origin to increase the accuracy of the coordinate system established. The further away from the origin the mapping area was the less accurate the coordinate system was due to the samples not being perfectly parallel with the crosshairs when designating the origin.

Along with trying to stay close to the origin, trying to use a distinct feature of the sample as a marker was another technique often used. This was necessary because even under ideal situations the coordinate system was often off by a micrometer or so and this could be alleviated by using a distinct feature in the sample to base the starting point of the map by. By combining these two techniques a relatively reliable method for generating precise and accurate maps could be implemented. An example of a marker used to refine a map can be seen below in Figure 22. It

should be noted that even though it was desirable to have the marker placed in the corner of the map, this was not always possible due to the geometry of the graphene coverage.

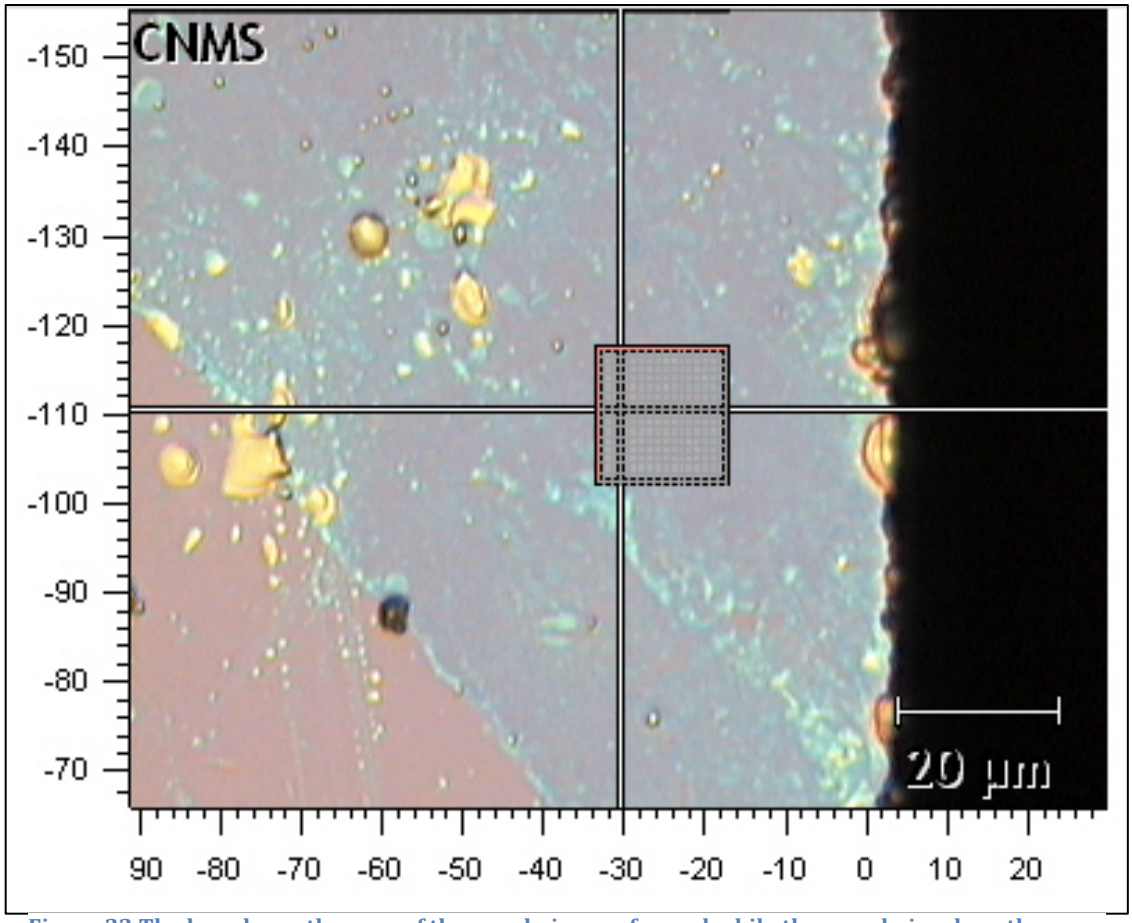

Figure 22 The box shows the area of the map being performed while the crosshairs show the point being measured at the particular time. More details on mapping will be discussed in the following section (Photo by author)

When a map is generated, the top left corner is the starting point. As can be seen in Figure 22 above, there is a slightly lighter blue dot right above the top left corner of the mapping box. This dot was then combined with the light blue section on the lower left corner to help place

the coordinates for the map on this sample. However, it should be noted that even though some markers were more convenient than others, having a consistent map size was the most important metric and no compromises were made to change this other than having uniform graphene coverage.

The last consideration taken into account was the quantity and quality of graphene in the area. As mentioned previously Si-SiO_2 with ~300nm thick SiO_2 allows graphene to be seen under normal white light conditions. By exploiting this feature and using a montage it is relatively easy to find an area of uniform graphene coverage that meets all the desired requirements. Figure 23 below shows an area of uniform graphene coverage being mapped. What can also be

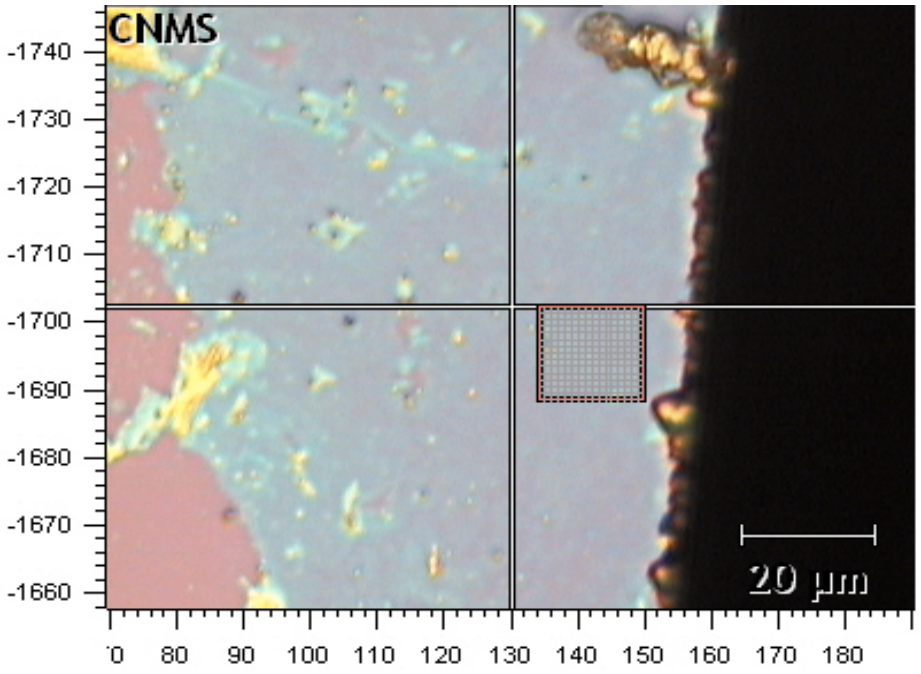

Figure 23 Shows an area being mapped that is uniform in color and therefore uniform in graphene quality and quantity. (Photo by author)

seen in Figure 23 is the graphene towards the right of the sample is much more uniform than the graphene and silicon (pinkish purple) on the left. Changes in color or holes in coverage generally mean damaged graphene or multiple layer graphene which is not desirable for this experiment. Being able to judge the graphene solely on its optical appearance to the human eye is not accurate enough to verify its condition.

5.4: Mapping Details and Raman Settings

In order to verify that the area is undamaged and is single layer graphene a single point Raman measurement is conducted. This measurement and all mapping measurements are conducted with a 633nm wavelength laser operating at 100% power (~1.2mW) with a 50x objective and a 10 second integration time. By conducting this measurement the quality of the graphene in question will be known and then the graphene surrounding the point of measurement can then be assumed to be of similar quality if it appears optically similar to the eye. However, the exact quality of the graphene will not be known completely until the map of the area has been completed, as small amounts of damage or doping are generally not able to be seen with a human eye. A Raman plot showing normal undamaged single layer graphene found in this experiment can be seen in Figure 24 below.

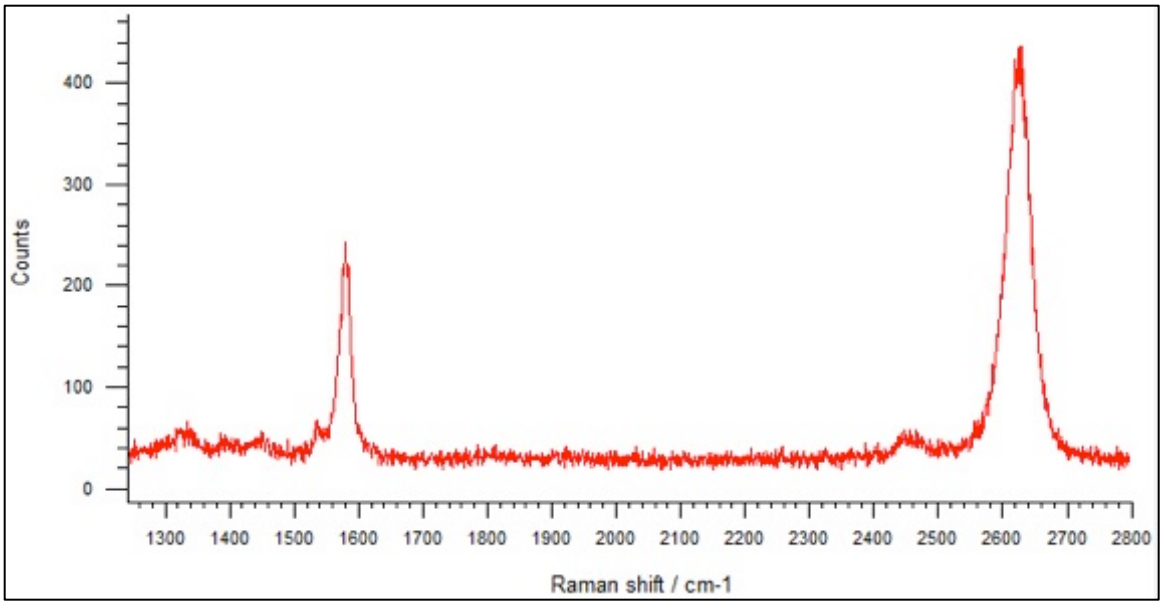

Figure 24 A Raman plot of undamaged single layer graphene. (Plot by author)

By checking to make sure that the point measured on each sample looks similar to the plot above and corresponds to an area that is optically similar, a mapping area for each sample was found. After a potential area was found, a map was then run. Each map was set up to measure a 15 μm by 15 μm area with a snaking pattern and a 1 μm step size which corresponds to 256 unique measurements. All the Raman settings were the same as described at the beginning of this section and each map took approximately 5 hours to run. Figure 25 below shows the settings imputed into the Renishaw software to conduct each map and the corresponding map that the input settings generated.

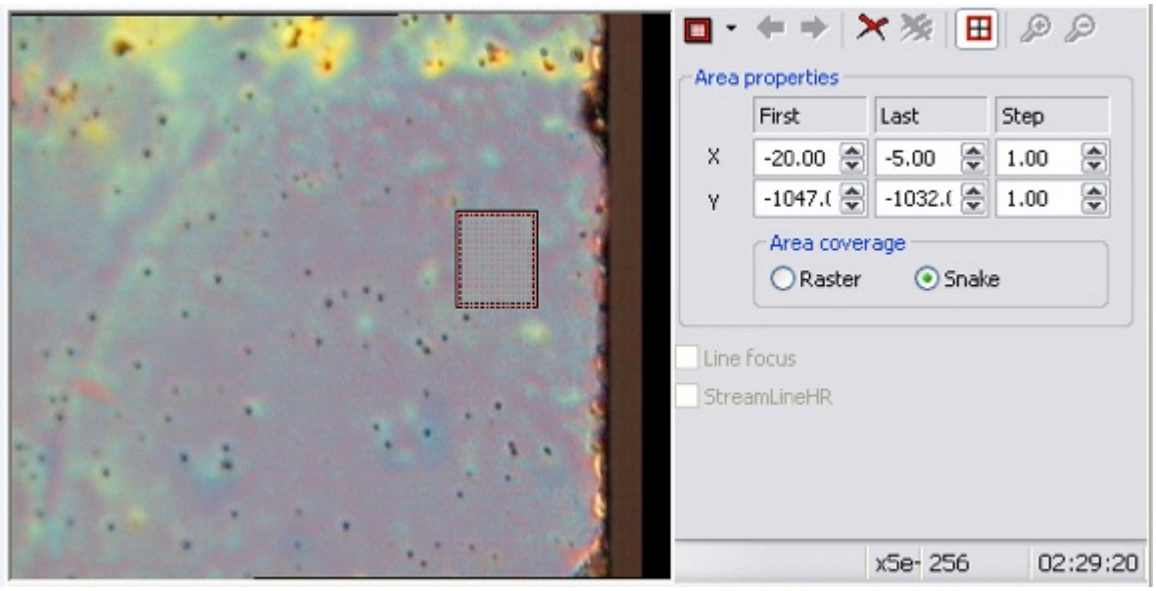

Figure 25 The map inputs and corresponding output can be seen. (Photo by author)

By repeating this process for each sample, a map for each sample could be generated with the same size and roughly the same quality. By carefully documenting each sample as described above, a map using the same physical area within a micrometer or less for each sample could also be found. This accuracy was estimated by comparing the map pictures of the pre- and post-irradiation samples. An example of this comparison can be seen in Figure 26 below. It should be noted that the area of the maps in Figure 26 are not the same due to distortion from editing the pictures so that they fit on the same picture, but if looked at carefully one can see that the top and bottom left corner which are the most important parts of the map display are on the same distinct features on each sample.

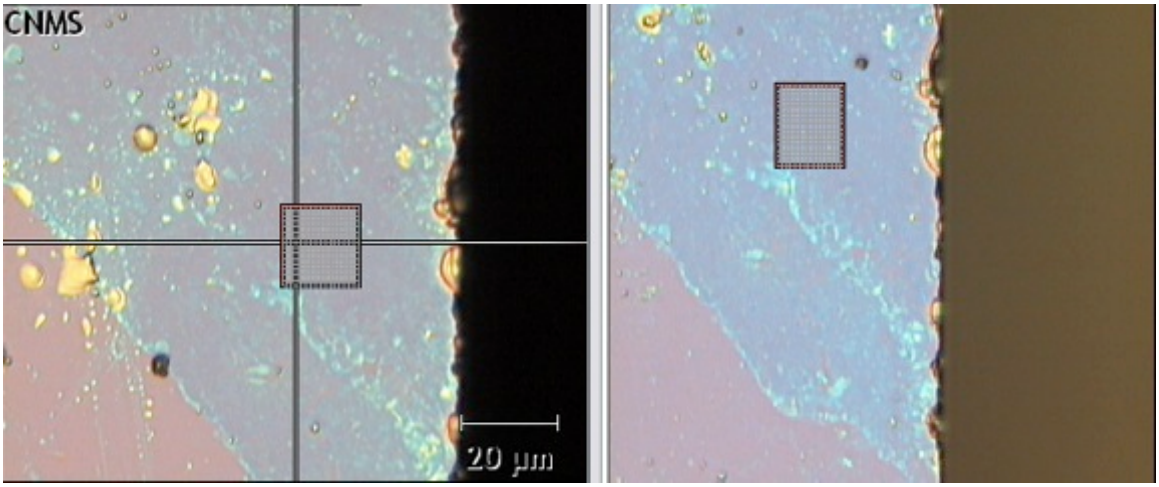

Figure 26 By repeating this comparison for each sample, the same area was able to be measured for each sample. Pre-irradiation is on the left, post-irradiation on the right. (Photo by author)

It can also be seen that after irradiation some of the coloration of the samples changed which made location of some of the distinct features more difficult. This is why it was imperative that a coordinate system and montage was used in conjunction with the distinct features.

5.5: Post Processing

As mentioned previously the high variability inherent in the graphene samples forced a mapping technique to be used. Each mapping measurement provided 256 unique measurements. This data was handled using the built-in software of the Renishaw Raman spectroscopy machine called WiRE and statistical analysis software called Origin. By using the curve-fitting feature in WiRE, the peak position, peak intensity, and width of the G (~1580cm^{-1}), D (~1350cm^{-1}) and DD (~2700cm^{-1}) bands could be calculated along with the ratio in intensities of the G/D and G/DD band. However

before calculating these metrics, outliers and peaks caused by cosmic background radiation had to be removed and this was done using the built in tools in WiRE. After calculating this data, the data could then be plotted spatially using the WiRE software to make plots such as those shown in Figure 27 below.

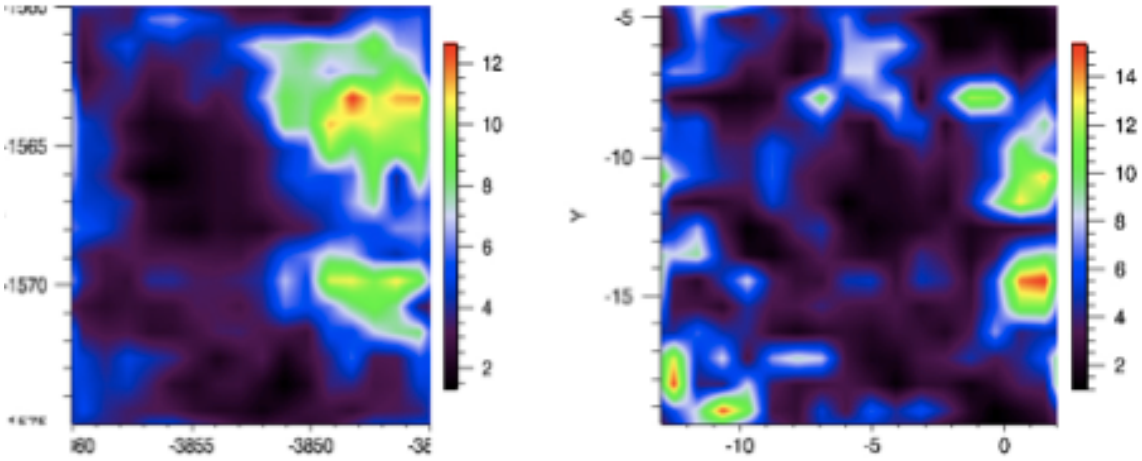

Figure 27 Shows the G/D ratio for a sample before (left). And after a 300 second irradiation (right). (photo by author)

Although these plots were useful for initial analysis there were a couple of issues with them. The first issue was the scale had to be unique for each plot as the change in range was significant enough to cause features to be indistinguishable or lost on one of the plots if the same scale was used on both. Due to this issue a different scale had to be used on each plot, which can be seen above in Figure 27. This caused comparisons between the two to be difficult and changes could not be easily seen. More importantly, there was no way to do any statistical analysis in the WiRE software so even if a change were to

be noticed, it was uncertain if this change was statistically relevant. To resolve this issue, Origin software was used to run statistics on the calculated data from WiRE. The 256 unique measurements for each metric were then averaged and the standard deviation was calculated, which was then assumed to be the variance. By calculating this data, all measurements related to a specific metric such as G/D band intensity could then be plotted on a single graph with the total fluence or time between measurements being on the X-axis. Examples of these plots will be shown in the following sections. An individual plot was then generated for heating samples, control samples and the HFIR irradiated samples. After these plots were generated, the linear regression, 95% confidence lines, 95% prediction lines and the coefficient of determination were all found for each metric using Origin.

The following sections will discuss these metrics and how they relate to the effects caused by irradiation. However, not all metrics showed a trend and some metrics such as intensities were used to calculate ratios only. Specifically the widths of the G, D, DD bands and the position of the D-band showed no noticeable trends and are not discussed.

6. Results and Conclusions

6.1 Gamma Samples

As discussed in section 4.5 the gamma facilities at the HFIR were used in order to try and de-couple the effects of the gamma rays from the neutrons. Unfortunately, an error occurred during the process and all the samples that were irradiated were destroyed to the point that the Raman signature was completely lost. An example of a Raman plot after gamma irradiation is shown below in Figure 28.

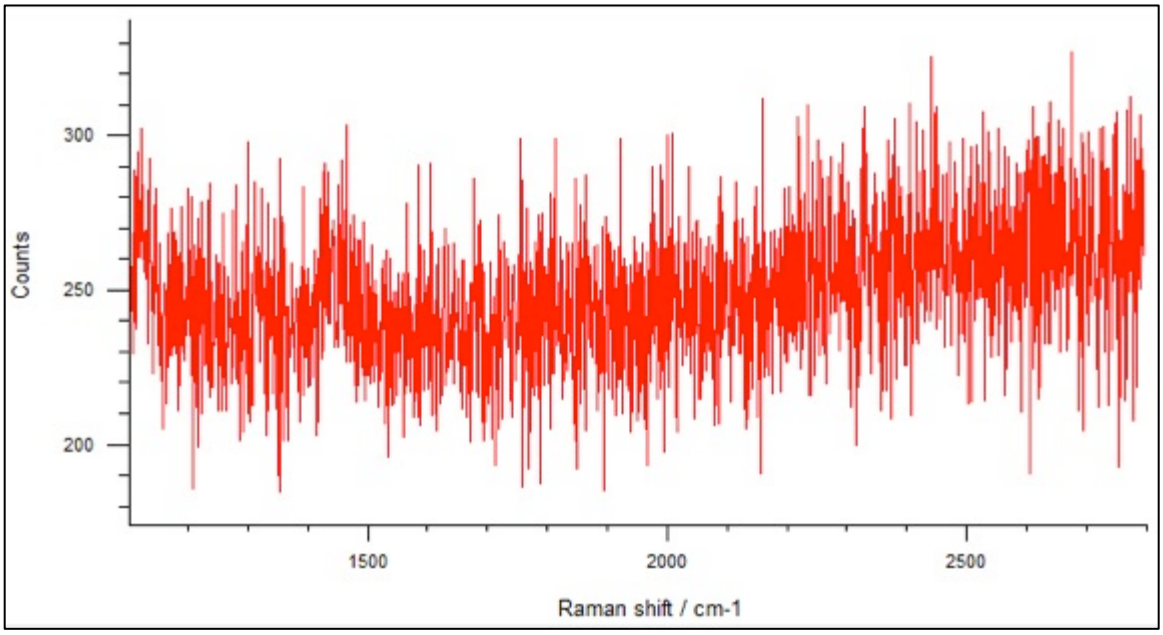

Figure 28 The Raman plot of a single point on a sample irradiated for 4440 seconds. Note the lack of peaks normally found on graphene even when damaged. (Plot by author)

It is not certain what exactly caused this issue, as all precautions were taken to try and simulate the same environment that the samples underwent during the neutron irradiations. This issue was not found in any of the neutron irradiated samples, but was found on the overwhelming majority of the points measured that were

irradiated by gamma rays including those that were irradiated the least amount of time. It is assumed that this severe amount of damage was related to the drastically longer irradiation times needed in order to simulate the same gamma doses found in the neutron irradiated samples. It is also possible that this effect is related to the damage of the containers that occurred due to the longer irradiation times as the containers changed in appearance after gamma irradiation as shown in Figure 29 below. It is also possible that these containers outgassed after being damaged and since graphene is extremely sensitive to any foreign covering, the Raman signal could have been lost due to the materials emitted from outgassing.

Since the containers did not undergo this change in coloration during neutron irradiations it can be reasoned that the dose rate and time are what is responsible for these changes and damage to the samples. Due to a lack of time and resources these measurements could not be repeated for this thesis although it is highly recommended that this experiment be repeated for any further work done in this field.

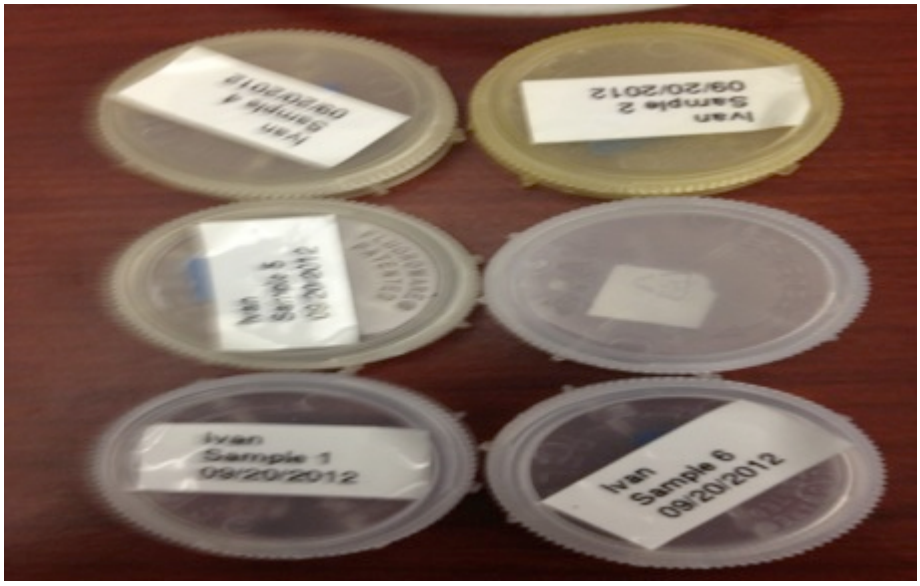

Figure 29 The HDPE containers can be seen after gamma irradiation. The bottom two samples were not irradiated and used as controls. (Photo by author)

6.2: Intensity Ratio of G/DD Band

One metric that was used for post- and pre-irradiation analysis was the ratio in intensities of the G to DD band. Changes in substrate can also affect this ratio, however the substrate used in this experiment was held constant for all measurements so this was not going to affect results. As shown in Figure 30 below, most of the samples measured had an average G/DD ratio of ~0.4 which roughly corresponds to single layer graphene. It can also be seen through the low coefficient of determination of 0.06 and the linear regression line drawn in red that the fluence had very little if any affect on the G to DD ratio. The 95% confidence and 95% prediction lines, which overlap in this case, can be seen as the

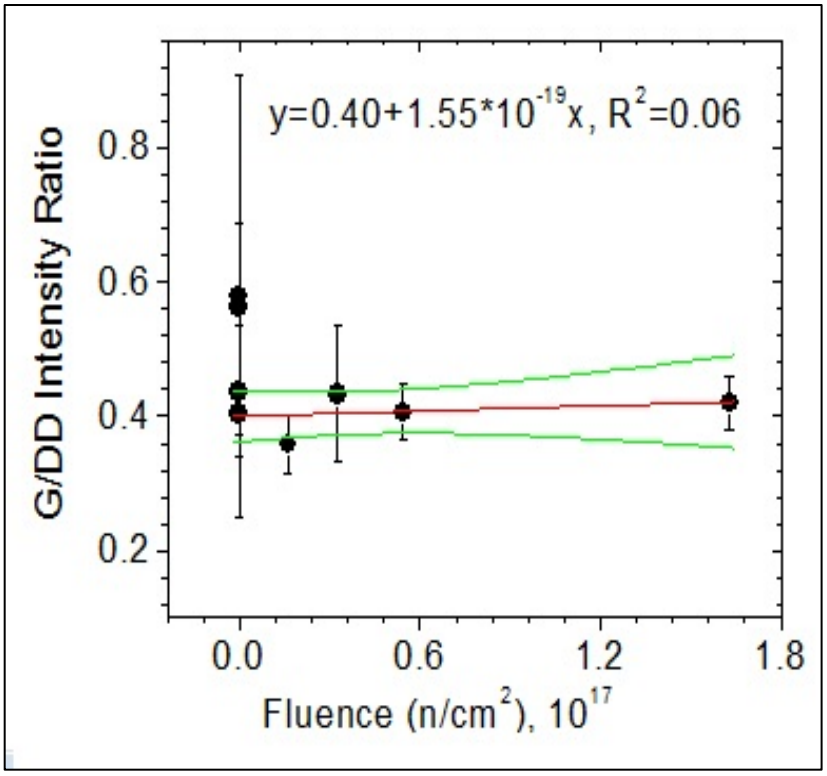

Figure 30 The G/DD band intensity is shown as a function of fluence. The equation used for this line is also shown above the plot along with R^2 the coefficient of determination. (Plot by author)

green lines above on the plot. The lack of change after irradiation makes intuitive sense as the amount of damage necessary to remove a layer of graphene is highly unlikely at this low of a fluence as the reaction cross section for carbon is too low. The control and heating samples also showed no change outside the sample variance, which is in agreement with the HFIR irradiated samples. As stated previously, this metric was primarily used to check the number of layers found in the samples, but was also used as a check to make sure the results had realistic conclusions.

6.3: Intensity Ratio of G/D Band

The ratio in intensities of the G to D-band are primarily used to tell the amount of disorder found in the system as Equation 1 in section 1.4 shows and the lower this ratio becomes the more disorder is present. However, this ratio is prone to the effects of doping as doping increases disorder as well. Since carbon has a low interaction cross-section for gamma rays, high-energy betas and neutrons, it is assumed that the change in the G/D ratio is primarily attributed to two types of dopants [19].

One type of doping that is assumed to be occurring takes place from the radiolysis of the water from humidity found in the samples. Radiolysis then produces products that could temporarily dope the sample, but would be removed as the water was removed from the sample due to heating. These products and the effects that they had on the graphene samples will be discussed further in the following section. Another type of doping occurs from the O_2 found in the atmosphere and can permanently dope the samples unless temperatures of 300℃ or greater are applied [36]. It is believed that this type of doping which can also be thought of as a soft etching process is partially responsible for the trends shown in Figure 31 below. It should be mentioned that the radiation the sample is exposed to must also contribute to this phenomena as well.

Figure 32 shows that heating or exposure to atmosphere alone do not change the G/D ratio in a substantial manner. It is assumed that ionizations from the radiation increase the amount of soft etching that can occur, but further measurements and more data will be needed for confirmation.

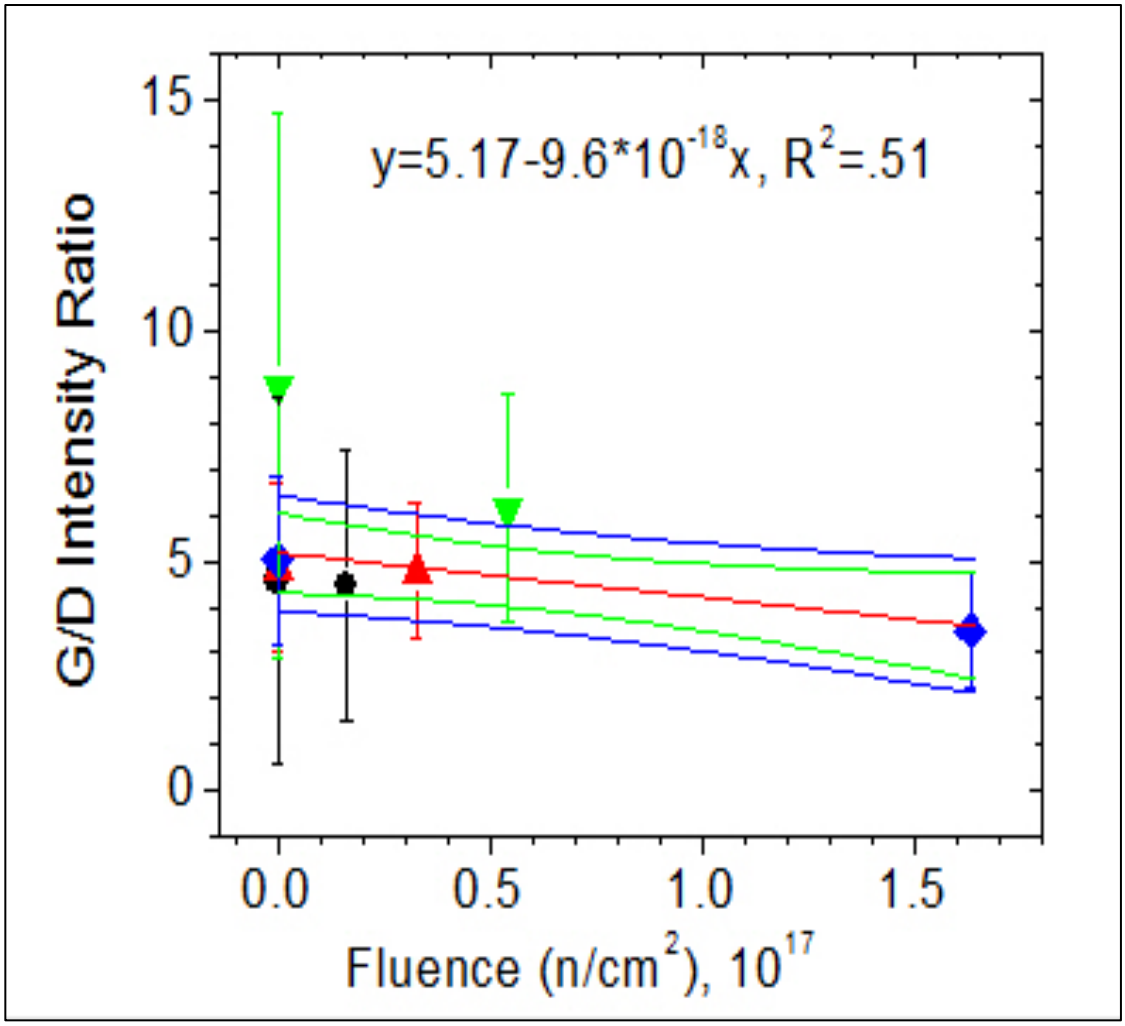

Figure 31 Each sample in this plot is colored uniquely to show clearly the change that it went through during irradiation. The blue lines show the 95% prediction lines while green show 95% confidence lines. (Plot by author)

Unlike the G/DD ratio, the G/D ratio has a much higher coefficient of determination at 0.51 showing a stronger

relationship between the amount of disorder and the total fluence. This data was also used to make Table 3 below which used the G/D ratios and Equation 1 to calculated the disorder distance shown.

Table 3 The data gathered from G/D measurements is shown

Sample	HFIR Time (sec)	Fluence (n/cm^2-sec)	Average Disorder Distance (nm)	G/D Average	Percent Change	Variance
1-Pre	0	0	176.59	4.58	0	3.97
1-Post	30	1.63E+16	172.47	4.47	-2.33	2.91
2-Pre	0	0	186.97	4.85	0	1.83
2-Post	60	3.27E+16	184.08	4.77	-1.55	1.48
3-Pre	0	0	339.23	8.80	0	5.88
3-Post	100	5.44E+16	236.25	6.13	-30.35	2.48
4-Pre	0	0	193.07	5.01	0	1.82
4-Post	300	1.63E+17	134.55	3.49	-30.31	1.26

The relatively high variances found in these measurements are attributed to the many different zones that are prone to doping. These zones are: The top layer of the single layer graphene, the top layer of the multiple layer graphene, the zone between the layers of graphene, the zone between the silicon dioxide and the single layer graphene and the zone between the silicon dioxide and the multilayered graphene. Some of these zones are only found

if multiple layers of graphene are present, but traces of multilayered graphene are present in the sample. It can also be seen in Table 3 above that the variance found in each sample decreases after irradiation. The reason why this is believed to occur is that there is a much more uniform doping found in the sample after irradiation compared to the uneven doping found prior. As mentioned previously this doping cannot solely be based off of the heating that occurs while the samples are irradiated or exposure to the atmosphere as both the heating and control sample shown in Figure 32 below showed no substantial changes unlike those found in the HFIR irradiated samples.

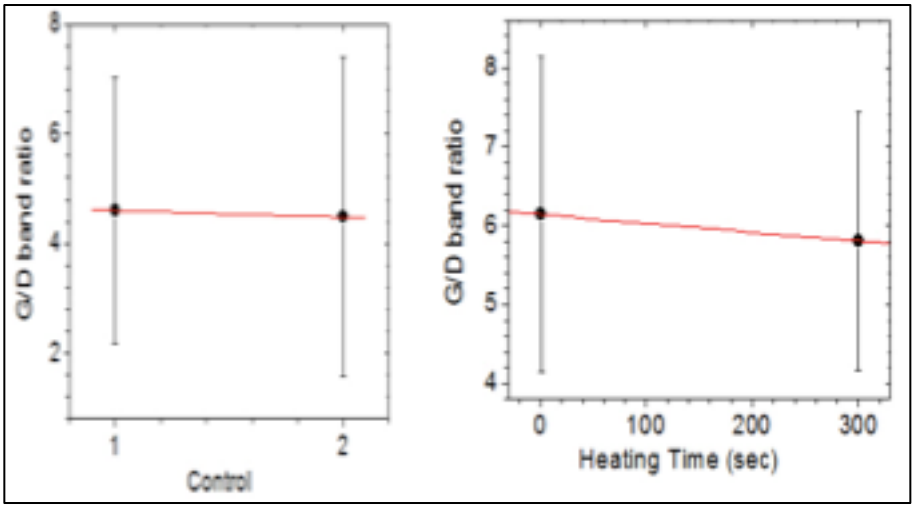

Figure 32 The lack of substantial change to either sample compared to the HFIR irradiated samples can be seen in the figure above. (Plot by author)

It can be seen in the figure above that the control sample had very little change in the G/D ratio and that this small change is still well within the variance of the sample. The heating sample shows a slight increase in

disorder, but again it is well within the variance and not as substantial as the changes found in the irradiated samples. The heating sample also had a slight decrease in variance as well, but this is not as significant as the change in variance found in the irradiated samples. These data reiterate that while heating is part of the soft etching process, it is not the sole reason why the etching is occurring in the irradiated samples and that this etching process must be assisted by the radiation.

6.4: Position Shift of G and DD Bands

The radiolysis of the water from humidity found in the samples and the products from radiolysis are believed to be temporarily doping the sample. Figure 33 below shows the

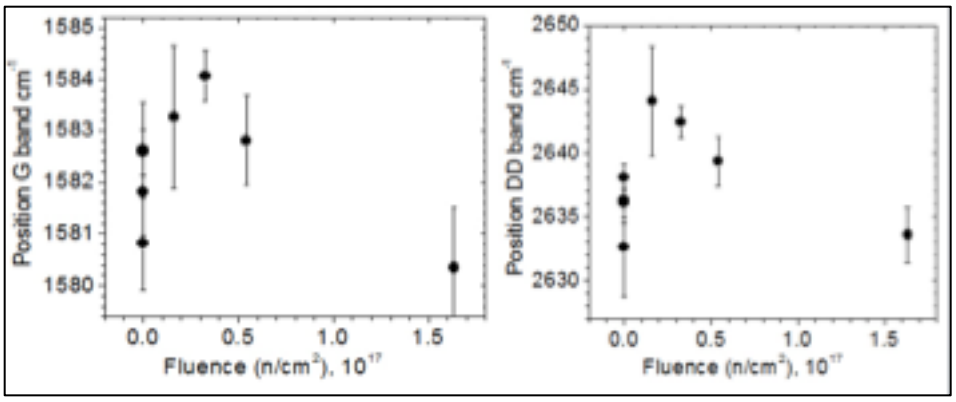

Figure 33 Both the G and DD bands exhibit a similar trend as can be seen above. (photo by author)

trends of the G and DD position which both increase temporarily due to doping, but then both decrease as the dopants are removed by the removal of water due to heating.

The radiolysis in this experiment is caused primarily by the gamma irradiation as thermal neutrons are often scattered by H_2O and are not responsible for significant amounts of radiolysis unless higher energy neutrons are used. Since the HFIR has a high amount of thermal neutrons and the fluences are relatively low in this experiment, neutrons are believed to not contribute substantially to this process.

Up to 46 different types of molecules and free radicals are produced by radiolysis however, many of them are short lived [37]. The longest living molecule that is believed to be responsible for the majority of the doping occurring to the graphene samples is H_20_2. To quantify the amount of production from radiolysis G-values are used. G-values are defined as the mean amount of a product produced in moles per 100 eV of energy absorbed. For H_2O_2 the G values are 1.06 for gamma irradiation and 0.0 for fast neutron irradiation [37]. Although fast neutrons can lead to the creation of radiolysis products such as OH, H, and H_2 it is not believed to generate significant amounts of H_2O_2 as shown by the G-value. This further reiterates that the main producer of dopants in this experiment is gamma irradiation.

These products are then bound to the water molecules present in the sample, which in turn cause the increase in G and DD band positions as shown above from doping. Since these products are bound to the water they are then removed as the water molecules are removed due to heating. The heating and control samples for both bands did not exhibit this trend showing the necessity of radiation for the production of the dopants.

Both band positions are not as sensitive to the etching process discussed in the previous section, but can be changed due to stress and strain of the sample [38-40]. In order for the samples to change in the manner shown above the stress and strain would have to be of a compressive manner which would be impossible from irradiation or heating [38-40]. Due to this it can be assumed that dopants alone are responsible for this process and that these dopants are generated by the irradiation that the sample underwent. This is promising because although the graphene did not sense the radiation directly the secondary effects of the radiation could be noticed. This makes graphene on $Si0_2$ a potential candidate for a radiation detector that could perhaps be tuned by varying the amount of water molecules due to humidity to detect different levels of radiation.

6.5: Recommendations

Although the initial results from this experiment look promising, several additional tests must be performed before graphene-based radiation detectors become a reality. The most important of these tests is redoing the gamma ray measurements. Without any data on the effects of gamma rays alone it is hard to determine what particle was most important to the production of dopants found in the graphene samples. It is also vital to know what role the gamma ray irradiation had in increasing the amount of disorder in the sample or if the disorder was all caused by the neutron irradiation.

Higher quality samples are desired as well. Although the samples used in this experiment were overall of high quality, the samples lacked uniform consistency, which made analysis more difficult. Along with uniformity, each sample did not have the same starting spectra before irradiation. Although most samples were as close as realistically possible to each other one sample in particular was not as close as the others and if more samples and time were available this sample would have been discarded. In future experiments great care should be taken to insure that all samples have as similar as realistically possible Raman spectra.

In addition to higher quality samples, more samples are also needed. For each fluence, it would be desirable to have at least two samples and a smaller gap between each fluence time would be preferable for both neutron and gamma irradiations. By having more samples measured, the validity of the initial results could be increased. More samples could also permit a wider range of fluence times.

Along with using graphene attached to $Si0_{2,}$ suspended graphene on TEM grids would also be a nice benefit to this research. By comparing the results of the two types of samples the importance of the humidity and doping zones to the doping process from irradiation could better be determined. By using a silicon nitride TEM grid longer irradiation times could also be possible. The samples on TEM grids could also be looked at further under a TEM, SEM or STEM microscope to see directly the damage caused by irradiation that was not possible during this experiment.

The effects of humidity on the results should be investigated further as well. By using a humidifier for different amounts of times on each sample, the importance of humidity could better be determined. Along with humidity, more samples should be heated for a longer range of times and temperatures to insure the significance of radiation to the doping process.

In addition to Raman spectroscopy measurements, tools such as an atomic force microscope (AFM), four point probe, spectroscopic ellipsometer and TEM/SEM/STEM microscopes could all be used to give more information on the condition of the graphene after irradiation.

Graphene doped with boron or other versions of functionalized graphene could also be used and designed for specific radiation detection purposes and tested. For example, boron-doped graphene would be much better at detecting thermal neutron irradiation. Increasing the water concentration trapped between it and the substrate by increasing the humidity that it is exposed to could also functionalize Graphene. With higher water concentration graphene could perhaps be more sensitive to detecting gamma irradiation through radiolysis.

6.6: Summary

Although the CVD grown graphene on a Si-SiO_2 substrate was not able to directly detect the effects of radiation, through secondary processes it was able to. Elevated amounts of soft etching and dopants which were both produced by irradiation could be detected through a change in the ratio of G/D band intensity and change of G and DD band positions. The trends found were verified by checking against the results of the heating and control samples.

None of the heating or control samples showed changes that were outside the variance of the samples and proved all the changes found were related to the effects of irradiation.

The O_2 found in the atmosphere combined with the radiation induced heating and ionizations are believed to be responsible for the trends in the ratio of G/D band intensity. This ratio was found to have a R^2 value of 0.51 showing statistical significance to the fluence time. The soft etching process from irradiation and exposure to O_2 is believed to be responsible for the permanent doping found in the samples, which consistently brought down the ratio of G/D band intensity.

Dopants produced by the radiolysis of water from gamma irradiation are believed to be responsible for the trends shown in the G and DD band positions. The positions increased and then decreased back to their original starting values after being irradiated for ~280 seconds. Primarily the radiolysis product of H_2O_2 is responsible for this trend and due to its dependence on water it is removed as the water is removed by evaporation from the radiation induced heating.

The ratio of G/DD band intensity for each sample was found not to change with irradiation. This shows that while there were changes to the graphene properties the

underlying structure was not affected. This result may be beneficial as it shows that graphene may be resilient to irradiation structurally.

With further testing and refinement it is thought that these trends can possibly be exploited for the use in a long-term gamma irradiation dosimeter without significant modification to how the graphene samples were tested. By using functionalized graphene such as boron-doped graphene, it is believed that a sensitive thermal neutron detector can be made as well. Although graphene is highly sensitive to a wide range of phenomena, these results show that with careful design it can be used in many applications in the nuclear engineering realm.

References

1. Iijima, S., *Single Wall Carbon Nanotube.* Nature, 1993. **603**: p. 363.
2. Singh, V., et al., *Graphene based materials: Past, present and future.* Progress in Materials Science, 2011. **56**(8): p. 1178-1271.
3. Geim, A.K. and K.S. Novoselov, *The rise of graphene.* Nat Mater, 2007. **6**(3): p. 183-191.
4. Congqin Miao, C.Z., Owen Liang, Ya-Hong Xie, *Chemical vapor deposition of graphene.* University of California, Los Angeles.
5. Malard, L.M., et al., *Raman spectroscopy in graphene.* Physics Reports, 2009. **473**(5-6): p. 51-87.
6. Ado Jorio, M.D., Riichiro Saito, Gene F. Dresselhaus, *Raman Spectroscopy in Graphene Related Systems*2011, Weinheim, Germany: Wiley-VCH. 351.
7. Gardiner, D.J., *Practical Raman Spectroscopy*2008, New York Springer-Verlag
8. Ferrari, A.C., *Raman spectroscopy of graphene and graphite: Disorder, electron-phonon coupling, doping and nonadiabatic effects.* Solid State Communications, 2007. **143**(1-2): p. 47-57.
9. Lucchese, M.M., et al., *Quantifying ion-induced defects and Raman relaxation length in graphene.* Carbon, 2010. **48**(5): p. 1592-1597.
10. Park, J.S., et al., *band Raman spectra of single, double and triple layer graphene.* Carbon, 2009. **47**(5): p. 1303-1310.
11. Vlassiouk, I., *Electrical and thermal conductivity of low temperature CVD graphene: the effect of disorder.* Nanotechnology, 2011. **22**(275716).
12. Slonczewski JC, W.P., *Band Structure Graphite.* Phys Rev, 1958: p. 109:272.
13. Novoselov, K.S.J.Y., Morozov SV, Stormer HL, Zeitler U, et al., *Experimental observation of quantum Hall Effect and Berry's phase in graphene. .* Science, 2007: p. 315:1379.
14. Li X, W.X., Zhang L, Lee S, Dai H. , *Chemically derived, ultrasmooth graphene nanoribbon semiconductors.* Science, 2008: p. 319:1229.
15. Schedin, F., et al., *Detection of individual gas molecules adsorbed on graphene.* Nat Mater, 2007. **6**(9): p. 652-655.
16. Gautam, M. and A.H. Jayatissa, *Gas sensing properties of graphene synthesized by chemical vapor deposition.* Materials Science and Engineering: C, 2011. **31**(7): p. 1405-1411.
17. Compagnini, G., et al., *Ion beam induced defects in graphene: Raman spectroscopy and DFT calculations.* Journal of Molecular Structure, 2011. **993**(1-3): p. 506-509.
18. Compagnini, G., et al., *Ion irradiation and defect formation in single layer graphene.* Carbon, 2009. **47**(14): p. 3201-3207.
19. E. H. Ahlgren, J.K., O. Lehtinen, A. V. Krasheninnikov, *Ion irradiation Tolerance of Graphene as studied by atomistic simulations.* Applied Physics Letters, April 12, 2012.

20. Mathew, S., et al., *The effect of layer number and substrate on the stability of graphene under MeV proton beam irradiation.* Carbon, 2011. **49**(5): p. 1720-1726.
21. Ilyin, A.M., E.A. Daineko, and G.W. Beall, *Computer simulation and study of radiation defects in graphene.* Physica E: Low-dimensional Systems and Nanostructures, 2009. **42**(1): p. 67-69.
22. Michael Foxe, E.C., H. Lamm, A. Majcher, C. Piotrowski, Isaac Childres, Amol Patil, Yong P. Chen, Igor Jovanovi, *Graphene-Based neutron detectors* IEEE Nuclear Science Symposium Conference, 2011. **352**.
23. Mike Foxe, G.L., Isaac Childres, Romaneh Jalilian, Caleb Roecker, John Boguski, Igor Jovanovic and Young P. Chen, *Detection of Ionizing Radiation Using Graphene Field Effect Transistors* IEEE Transactions on Nanotechnology 2012. **581**: p. 11.
24. Nam, I.W., H.K. Lee, and J.H. Jang, *Electromagnetic interference shielding/absorbing characteristics of CNT-embedded epoxy composites.* Composites Part A: Applied Science and Manufacturing, 2011. **42**(9): p. 1110-1118.
25. Potts, J.R., et al., *Graphene-based polymer nanocomposites.* Polymer, 2011. **52**(1): p. 5-25.
26. Ouyang, Y., *A simple method for achieving surface-enhanced Raman Scattering of single - layer and few - layer graphene.* Journal of Molecular Structure (2012), 2012.
27. *Table of Nuclides*. 2000 5-20-12]; Available from: http://atom.kaeri.re.kr/ton/index.html.
28. Blake, P., et al., *Making Graphene Visible.* Applied Physics Letters, 2007. **91**.
29. Leconte, N., et al., *Damaging Graphene with Ozone Treatment: A Chemically Tunable Metal–Insulator Transition.* ACS Nano, 2010. **4**(7): p. 4033-4038.
30. Sims, T.M.a.J.H.S., *High Flux Isotope Reactor (HFIR) Experiment Facilities and Capabilities.* ORNL, 1979.
31. Cheverton, R.D.a.T.M.S., *HFIR Core Nuclear Design.*, in *ORNL*1971.
32. ORNL, *High Flux Istope Reactor (HFIR) User Guide: A guide to in-vessel irrdiations and experiments*, 2011, DOE
33. Dr. Randy Hobbs, *Dr. David Chandler, David Glasgow*: 2012.
34. Clavel, M., et al., *Study of annealing temperature influence on the performance of top gated graphene/SiC transistors.* Solid-State Electronics, 2012. **71**(0): p. 2-6.
35. Duraia, E.-S.M., Z. Mansurov, and S. Tokmoldin, *Formation of graphene by the thermal annealing of a graphite layer on silicon substrate in vacuum.* Vacuum, 2011. **86**(2): p. 232-234.
36. Ryu, S., et al., *Atmospheric Oxygen Binding and Hole Doping in Deformed Graphene on a SiO2 Substrate.* Nano Letters, 2010. **10**(12): p. 4944-4951.
37. Ishigure, K., et al., *Radiolysis of high temperature water.* Radiation Physics and Chemistry, 1995. **46**(4–6, Part 1): p. 557-560.
38. Bissett, M.A., et al., *Effect of Domain Boundaries on the Raman Spectra of Mechanically Strained Graphene.* ACS Nano, 2012. **6**(11): p. 10229-10238.

39. Mohiuddin, T.M.G., et al., *Uniaxial strain in graphene by Raman spectroscopy: G peak splitting, Grüneisen parameters, and sample orientation.* Physical Review B, 2009. **79**(20): p. 205433.
40. Komurasaki, H., et al., *Layered Structures of Interfacial Water and Their Effects on Raman Spectra in Graphene-on-Sapphire Systems.* The Journal of Physical Chemistry C, 2012. **116**(18): p. 10084-10089.